remote sensing

MDPI

Article

Simultaneous Time-Varying Vibration and Nonlinearity Compensation for One-Period Triangular-FMCW Lidar Signal

Rongrong Wang [1,2], Bingnan Wang [1,*], Maosheng Xiang [1,2], Chuang Li [3], Shuai Wang [1,2] and Chong Song [1,2]

[1] National Key Laboratory of Microwave Imaging Technology, Aerospace Information Research Institute, Chinese Academy of Sciences, Beijing 100190, China; wrr0817@126.com (R.W.); xms@mail.ie.ac.cn (M.X.); wangshuai161@mails.ucas.edu.cn (S.W.); songchong18@mails.ucas.edu.cn (C.S.)
[2] School of Electronics, Electrical and Communication Engineering, University of Chinese Academy of Sciences, Beijing 100049, China
[3] National Engineering Laboratory for Offshore Oil Exploration, School of Information and Communications Engineering, Xi'an Jiaotong University, Xi'an 710049, China; chuangli@xjtu.edu.cn
* Correspondence: wbn@mail.ie.ac.cn

Abstract: Frequency modulation continuous wave (FMCW) Lidar inevitably suffers from vibration and nonlinear frequency modulation, which influences the ranging and imaging results. In this paper, we analyze the impact of vibration error coupled with nonlinearity error on ranging for FMCW Lidar, and propose a purely theoretical approach that simultaneously compensates for time-varying vibration and nonlinearity in one-period triangular FMCW (T-FMCW) signals. We first extract the localized characteristics of dechirp signals in time-frequency domain by using a second-order synchro-squeezing transform (second-order SST), and establish an instantaneous ranging model based on second-order SST which can characterize the local distributions of time-varying errors. Second, we estimate the nonlinearity error by using time-frequency information of an auxiliary channel and then preliminarily eliminate the error from the instantaneous measurement range. Finally, we construct a particle filtering (PF) model for T-FMCW using the instantaneous ranging model to compensate for the time-varying vibration error and the residual nonlinearity error, and calculate the range of target by using triangular symmetry relations of T-FMCW. Experimental tests prove that the proposed method can accurately estimate the range of target by compensating for the time-varying vibration and the nonlinearity errors simultaneously in one-period T-FMCW signal.

Keywords: time-varying vibration; nonlinearity compensation; instantaneous ranging model; second-order SST; PF model; triangular FMCW Lidar

Citation: Wang, R.; Wang, B.; Xiang, M.; Li, C.; Wang, S.; Song, C. Simultaneous Time-Varying Vibration and Nonlinearity Compensation for One-Period Triangular-FMCW Lidar Signal. *Remote Sens.* **2021**, *13*, 1731. https://doi.org/10.3390/rs13091731

Academic Editor: Piotr Samczynski

Received: 19 March 2021
Accepted: 26 April 2021
Published: 29 April 2021

1. Introduction

Triangular frequency modulation continuous wave (FMCW) Lidar system can achieve long range detection with low power cost, and therefore it is widely used in target detection, range measurement, velocity measurement, air turbulence detection synthetic aperture Lidar, and three-dimensional (3D) imaging [1]. We focus on the application of triangular FMCW Lidar to range measurement in this paper. The FMCW Lidar source can be obtained by directly modulating the laser source or using an external modulator, and we use the second approach. To be specific, we first generate a single-frequency laser signal and a microwave frequency modulation signal, and apply an external modulator to the laser signal by using the driven signal to obtain the FMCW laser source [2]. The wavelength of laser is 1.55 µm, which is supposed to be eye-safe in long range detection [3,4]. We then apply a coherent detection mechanism to receive the reflected signals, which can reduce the burden of signal acquisition. However, the FMCW Lidar signals inevitably suffer from two major errors in range measurement. The first error source is a nonlinear frequency modulation error introduced by microwave modulation and photoelectric conversion to the transmitted FMCW Lidar signal, and it can lead to energy diffusion and affects the image quality [5]. The second error source is vibrations generated between the Lidar platform and the target. Unfortunately, the coherent detection mechanism is very sensitive to vibrations because the wavelength of lasers is extremely small [6]. Even a small vibration error will introduce great errors to the ranging result. The vibration error coupled with the nonlinearity error has a relevant contribution in the overall error budget in the ranging and imaging results, which leads to problems such as spectrum energy diffusion, main lobe broadening, and side lobe lifting [7]. Therefore, compensating for the influences of vibrations coupled with nonlinearity on triangular FMCW Lidar signals is important for high-resolution range measurement.

Vibration compensation methods are mainly used in frequency-scanning interferometry (FSI) which has a similar principle with FMCW in the application of ranging. There are two main approaches to compensate for vibration errors. The first approach eliminates the vibration errors by adding hardware devices such as lasers or speed detection modules. Kakuma et al. [8] adopted two vertical cavity surface emitting lasers with opposite frequency sweep directions for ranging and eliminated the vibration errors by averaging the phase shift of two measurement echoes. Krause et al. [9] added a single-frequency laser to the basic FSI system and eliminated the vibration error by synthesizing the echoes obtained from the two lasers. Yang et al. [10] established a dual laser ranging system in which two lasers transmit frequency modulation signals in opposite directions of frequency scan simultaneously, and thereby eliminated slow vibration errors by combining consecutive echoes obtained from the lasers. Martinez et al. [11] proposed a vibration compensation method based on four-wave frequency mixing which uses a tunable laser and a single-frequency laser to generate two frequency scanning signals with opposite frequency sweep directions, and then compensated for the vibration errors by using triangular symmetry relations of the echoes. The above methods with additional lasers can effectively compensate for the vibration and nonlinearity errors, but they generally have asynchronous problems between multiple lasers. The second approach can reduce the complexity of system design compared with the first approach. It usually acquires long observation time by collecting consecutive echoes, and then establishes mathematical relations of these echoes to suppress vibration errors and estimate the range of target. For instance, Swinkels et al. [12] indicated that the range measurement could be performed with only one laser, in which several subsequent measurements of up and down frequency sweep would be used to compensate for the vibration errors. However, this method cannot reduce the sensitivity to severe vibrations in an industrial environment. Tao et al. [13] proposed a movement error compensation method by using a Kalman filter technique which only needs one tunable laser driven by up and down optical frequency scanning. This method achieved high-precision in range measurement by using consecutive echoes. Jia et al. [14] applied a time-varying Kalman filter to the basic range measurement system and improved the performance of range measurement, and it needs a long observation time to provide enough measurement results. However, 3D imaging adopts the laser scanner for dynamic range measurement, in which the measurement time of each observation spot is short [15]. As we usually obtain one measurement result from one-period echo of the FMCW ranging system, this means it cannot directly provide enough measurement results for the vibration compensation methods mentioned above. Thus, we need to compensate for the vibration errors by using one-period FMCW signals. The vibration error can be removed in one period of triangular FMCW by measuring the Doppler shift of the beat frequency for up-chirping and down-chirping state when the velocity of vibration can be assumed to be constant [16]. However, in FMCW lidar systems, especially those installed on airborne platforms, the engine and other mechanical equipment generate much more severe vibrations with frequencies of up to several hundred hertz. In this case, the velocity of vibration is time-varying for fast vibrations, which degrades the performance of the Doppler shift method.

Besides the vibration errors, the other error source of the dechirp signal is the nonlinearity errors which are compensated by two main approaches. The first approach monitors the time-varying optical frequency in real time by setting an auxiliary channel and regards its output as a clock signal to sample the measured dechirp signal with an equal optical frequency interval rather than an equal time interval during data acquisition. However, the maximum detectable range is limited by the range of the auxiliary channel to satisfy the Nyquist sampling theorem [17]. The other approach suppresses the nonlinearity after data acquisition which is free of the range limitation. The Hilbert transform can be used to estimate the nonlinear frequency of the reference dechirp signal in the auxiliary channel and then compensate for the nonlinearity of the measured dechirp signal using the reference information [18], but it needs to conduct phase unwrapping. Anghel et al. presents a nonlinearity compensation method for FMCW radars based on high-order ambiguity functions (HAF) and temporal resampling. HAF is used to estimate the nonlinearity polynomial coefficients which are then applied to the measurement signal by temporal resampling [19]. Yüksel et al. [20] converts the time-varying phase of the reference dechirp signal into amplitude change and estimates the nonlinear frequency by detecting the amplitude envelope. The nonlinearity can be compensated by resampling the measured dechirp signal with an equal optical frequency sampling interval, but it needs the noise level of the data to be quite low.

In general, the vibration error is usually coupled with nonlinearity errors which can significantly reduce the ranging accuracy. Lu et al. added a laser Doppler velocimetry module on the basis of ranging system. The velocimetry module is composed of a single-frequency laser and acoustic optical modulators, which can obtain the Doppler offset of the measured target and then compensate for the vibration error. In addition, the above system uses an auxiliary channel to produce clock signals to resample the dechirp signals of the measurement channel and reduces the interference of nonlinearity error on ranging [21]. However, resampling the measurement dechirp signals by regarding the reference signals as clock signals introduces a nonlinear term to the real time. Therefore, Lu et al. [22] introduced a phase-locked loop on the basis of the above ranging system and effectively solved the nonlinear problem of the clock signals. This method can simultaneously eliminate vibration error and nonlinearity error and has a remarkable prospect in the applications of ranging, but it needs two lasers.

Motivated by the above methods, we establish an instantaneous ranging model based on the second-order synchro-squeezing transform (second-order SST) and present a time-varying vibration and nonlinearity compensation method based on a particle filtering (PF) model using the instantaneous ranges. Since the second-order SST can depict local characteristics of strongly modulated signals, it is useful to characterize the small perturbations of the dechirp signals in time-frequency domain caused by severe time-varying vibration and nonlinearity errors [23]. Thus, the instantaneous ranging model can characterize the local distributions of time-varying errors. We first use the instantaneous ranging model to estimate the nonlinearity errors in the auxiliary channel and use them to preliminarily compensate for the nonlinearity errors in the measurement range. After that, the measurement range still suffers from vibration errors and residual nonlinearity errors. The PF is a useful tool to estimate the optimal state of system by selecting a group of random samples in the state space to approximate the probability density function, and the samples reflecting the state of system are called "particles" [24]. Thanks to the instantaneous ranging model, we can obtain sufficient measurement ranges from only one-period triangular FMCW (T-FMCW) Lidar signals for the PF. Thus, we use the instantaneous range to construct a PF model for T-FMCW by which we can filter out the vibration errors, the residual nonlinearity errors, and noise from the measurement ranges. Therefore, the proposed method can simultaneously compensate for the nonlinearity errors and the fast vibration errors in a one-period T-FMCW Lidar signal and is robust to noise.

The remainder of this paper is organized as follows. In Section 2, we derive the impact of vibration coupled with nonlinearity on FMCW Lidar ranging. In Section 3, we establish an instantaneous ranging model based on the second-order SST and introduce the time-varying vibration and nonlinearity compensation method for FMCW Lidar based on the PF model and the instantaneous ranging model. In Section 4, we use four experimental tests to verify the effectiveness of the proposed method to simultaneously compensate for the time-varying vibration and nonlinearity in point target and 3D target imaging. In Section 5, we discuss the advantages and further applications of the proposed method. At last, we provide the conclusions in Section 6.

2. Analysis of Ranging Principle for FMCW Lidar

This section is divided into two parts. The first subsection describes the process of ideal coherence detection of FMCW Lidar, and the second subsection analyzes the influence of time-varying vibration coupled with nonlinearity on ranging.

2.1. Ideal Coherent Detection Process

The coherent detection of FMCW Lidar includes the following steps. First, the Lidar transmits frequency modulation signals, and the transmitted signals are reflected by the target. Then, we can obtain dechirp signals of the transmitted signals and the reflected echoes by heterodyne coherent detection of the receivers [25]. Finally, the dechirp signals are transformed into frequency domain, and the range of target can be calculated by using the frequency spectrum [26,27].

Figure 1 shows the schematic diagram of the dechirp process, in which Figure 1a represents the transmitted frequency and Figure 1b represents the dechirp frequency after coherent detection process. Since the dechirp frequencies of the close range and the long range are different, the coherent detection of an FMCW Lidar system can distinguish the close range and the long range compared with the fiber range. The fiber range means an artificial range introduced by fiber in the FMCW Lidar system. In Figure 1, Δr represents the range difference between the close range and the long range.

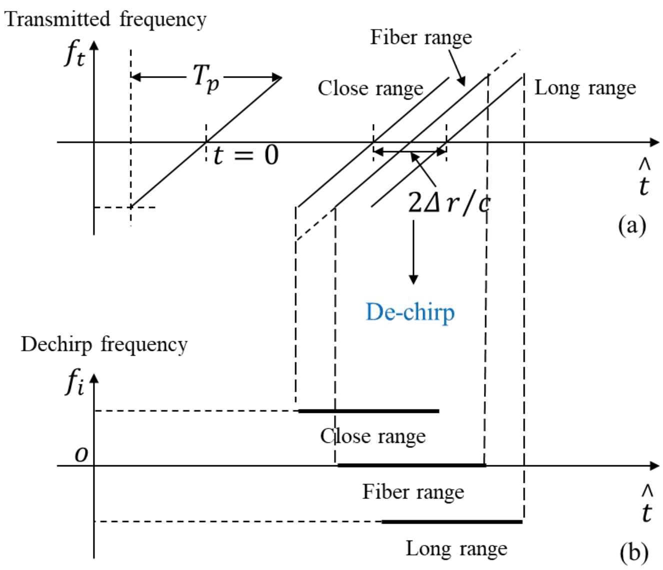

Figure 1. The schematic diagram of dechirp process: (**a**) the transmitted frequencies, (**b**) the dechirp frequency after coherent detection process.

The ideal transmitted signal of FMCW Lidar is expressed as

$$s_t(t) = w(t) \exp\left[j2\pi\left(f_c t + 0.5Kt^2\right)\right], \quad (1)$$

where $s_t(t)$ is the transmitted signal; f_c is the carrier frequency; $w(t)$ is the envelope of signal; and K is the frequency modulation rate.

The reflected echoes at target range R_d and the transmitted signal passing through the delay fiber at range R_f can be expressed as

$$\begin{cases} s_{Rd}(t) = w\left(t - \frac{2R_d}{c}\right) \exp\left\{ j2\pi \left[f_c\left(t - \frac{2R_d}{c}\right) + 0.5K\left(t - \frac{2R_d}{c}\right)^2 \right] \right\} \\ s_{Rf}(t) = w\left(t - \frac{2R_f}{c}\right) \exp\left\{ j2\pi \left[f_c\left(t - \frac{2R_f}{c}\right) + 0.5K\left(t - \frac{2R_f}{c}\right)^2 \right] \right\} \end{cases}, \tag{2}$$

where $s_{Rd}(t)$ and $s_{Rf}(t)$ are the reflected echoes at range R_d and the transmitted signal passing through delay fiber at range R_f, respectively; and c is the velocity of light.

Then, the dechirp signal is obtained by coherently mixing the two signals shown in Equation (2):

$$\begin{aligned} s_{if}(t) &= s_{Rf}(t) s_{Rd}{}^*(t) \\ &= w\left(t - \frac{2R_d}{c}\right) \exp\left[j2\pi \left(f_c \frac{2(R_d - R_f)}{c} + Kt\frac{2(R_d - R_f)}{c} - 0.5K\left(\frac{2(R_d - R_f)}{c}\right)^2 \right) \right] \end{aligned} \tag{3}$$

where $s_{if}(t)$ is the dechirp signal; and * represents the conjugate operator. The envelope will be ignored in the following section, and the second-order term of the echo delay in the phase is ignored since the echo delay is small. Define $R_0 = R_d - R_f$, and $\tau = 2R_0/c$ is the time delay of R_0. Then, the above equation can be simplified as

$$\begin{aligned} s_{if}(t) &= \exp\left[j2\pi \left(f_c \frac{2(R_d - R_f)}{c} + Kt\frac{2(R_d - R_f)}{c} \right) \right] \\ &= \exp\left[j2\pi \left(f_c \frac{2R_0}{c} + Kt\frac{2R_0}{c} \right) \right] = \exp[j2\pi(f_c\tau + Kt\tau)] \end{aligned} \tag{4}$$

By applying Fourier transform to Equation (4), we can obtain the target range by using the following Equation

$$R_d = R_0 + R_f = \frac{f_0 c}{2K} + R_f, \tag{5}$$

where $f_0 = K\tau$ is the ideal dechirp frequency of R_0.

2.2. Impact of Vibration Coupled with Nonlinearity on FMCW Lidar Ranging

The Lidar system inevitably introduces nonlinearity error to the transmitted FMCW signals [28]. When there is a nonlinear phase $e(t)$, the transmitted signal with nonlinearity can be obtained by substituting $e(t)$ into the ideal transmitted signal shown by Equation (1):

$$s_{te}(t) = \exp\left[j2\pi \left(f_c t + 0.5Kt^2 \right) + je(t) \right], \tag{6}$$

where $s_{te}(t)$ represents the transmitted signal with nonlinear phase. The reflected echo with nonlinearity is regarded as the transmitted signal containing time delay, which can be expressed as

$$s_{re}(t) = w(t - \tau) \exp\left\{ j2\pi \left[f_c(t - \tau) + 0.5K(t - \tau)^2 \right] + je(t - \tau) \right\}, \tag{7}$$

The dechirp signal with nonlinearity is obtained by coherently mixing the transmitted signal and the reflected echo:

$$s_{ife}(t) = \exp\{ j2\pi(f_c\tau + Kt\tau) + j[e(t) - e(t - \tau)] \}, \tag{8}$$

where $e(t) - e(t - \tau)$ is the nonlinearity error of the dechirp signal, which contains quadratic or higher-order components [29]. As shown in Equation (8), the spectrum of the dechirp signal is the convolution of the spectrum of an ideal dechirp signal and the spectrum of the nonlinearity term, which leads to energy diffusion and affects the image quality [30,31].

Then, we derive the influence of time-varying vibration coupled with nonlinearity on FMCW Lidar ranging. Figure 2 shows the influence of vibrations and nonlinearity on the ranging process. As shown in Figure 2, the transmitted beam contains nonlinear frequency, while the received beam contains both the nonlinear frequency and the Doppler frequency introduced by vibration. Therefore, the instantaneous phase of the dechirp signal is related not only to the nonlinearity of the transmitted signal but also to the Doppler frequency introduced by the vibration error [32].

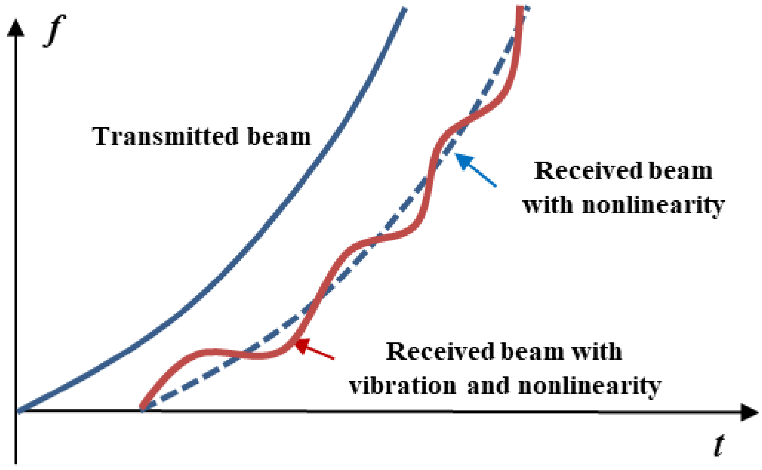

Figure 2. Influence of time-varying vibration coupled with nonlinearity on ranging.

The ideal time delay τ equals to $2R_0/c$. When the platform or the target has relative vibration, the constant τ will be denoted as a time-varying time delay $\tau(t)$ that equals to $2R(t)/c$. $R(t)$ is the instantaneous range of a target with vibration which can be expressed as

$$R(t) = R_0 + \int^t v(t')dt', \tag{9}$$

where $v(t)$ is the time-varying velocity of vibration. Doppler frequency shift will be introduced into the dechirp frequency due to the presence of $v(t)$, and we denote $2v(t)/c$ as $\tau'(t)$ which is regarded as the normalized Doppler frequency shift.

We define $f_t(t)$ as the transmitted frequency of the transmitted signal shown by Equation (6), and it can be expressed as

$$f_t(t) = f_c + Kt + f_e(t). \tag{10}$$

where $f_e(t)$ represents the nonlinear frequency. Then, we take the vibration error into consideration. The instantaneous phase of the dechirp signal with the coupling vibration and nonlinearity errors can be obtained by integrating the transmitted frequency shown in Equation (10), which is expressed as

$$\begin{aligned} \phi(t) &= \int_{t-\tau(t)}^{t} 2\pi f_t(t')dt' = \int_{t-\tau(t)}^{t} 2\pi[f_c + Kt' + f_e(t')]dt' \\ &\approx 2\pi(f_c + Kt)\tau(t) + \int_{t-\tau(t)}^{t} 2\pi f_e(t')dt' \end{aligned} \tag{11}$$

in which we ignore the high-order term of $\pi K\tau(t)^2$.

Then the corresponding instantaneous frequency is obtained by taking the derivative of phase shown in Equation (11):

$$\begin{aligned} \widetilde{f}(t) &= \frac{1}{2\pi}\frac{d[\phi(t)]}{dt} \\ &= (f_c + Kt)\tau'(t) + K\tau(t) + f_e(t) - f_e[t-\tau(t)][1-\tau'(t)] \\ &= \{f_c + Kt + f_e[t-\tau(t)]\}\tau'(t) + K\tau(t) + f_e(t) - f_e[t-\tau(t)] \end{aligned} \tag{12}$$

We expand the function $f_e[t-\tau(t)]$ about t using Taylor series expansion:

$$\begin{aligned} f_e[t-\tau(t)] &= \sum_{n=0}^{\infty} \frac{f_e{}^{(n)}(t)}{n!}[-\tau(t)]^n \\ &= f_e(t) - f_e'(t)\,\tau(t) + \sum_{n=2}^{\infty} \frac{f_e{}^{(n)}(t)}{n!}[-\tau(t)]^n \\ &= f_e(t) - f_e'(t)\,\tau(t) + O\left[\tau(t)^2\right] \end{aligned} \tag{13}$$

where $O\left[\tau(t)^2\right]$ represents the second- and higher-order terms $\sum_{n=2}^{\infty} \frac{f_e{}^{(n)}(t)}{n!}[-\tau(t)]^n$ and $f_e{}^{(n)}(t)$ is the n-th-order derivative of $f_e(t)$. Then we substitute Equation (13) into Equation (12), and the instantaneous frequency can be rewritten as

$$\begin{aligned} \widetilde{f}(t) &= \left\{f_c + Kt + f_e(t) - f_e(t)\tau(t) + O\left[\tau(t)^2\right]\right\}\tau'(t) + K\tau(t) + f_e'(t)\tau(t) - O\left[\tau(t)^2\right] \\ &= [f_c + Kt + f_e(t)]\tau'(t) + [K + f_e'(t)]\tau(t) + O\left[\tau(t)^2\right]\tau'(t) - O\left[\tau(t)^2\right] - f_e(t)\tau(t)\tau'(t) \\ &\approx [f_c + Kt + f_e(t)]\tau'(t) + [K + f_e'(t)]\tau(t) \end{aligned} \tag{14}$$

where $f_t'(t)$ is the first-order derivative of $f_t(t)$. The detection range $R(t)$ between the target range and the fiber range is usually from several meters to several hundred meters, and the time delay $\tau(t)$ is usually small in the Lidar system. If the detection range is 100 m, $\tau(t)$ will be on the order of magnitude 10^{-7}, and $\tau'(t)$ is on the order of magnitude 10^{-9}. Because K is on the order of magnitude 10^{11} and f_c is on the order of magnitude 10^{14}, the first two terms $[f_c + Kt + f_e(t)]\tau'(t) + [K + f_e'(t)]\tau(t)$ are much larger than the high-order terms $O\left[\tau(t)^2\right]\tau'(t) - O\left[\tau(t)^2\right] - f_e(t)\tau(t)\tau'(t)$. Therefore, we ignored the high-order terms and the truncation error is negligible.

By combining Equations (9) and (14), the instantaneous frequency of the dechirp signal can be rewritten as

$$\widetilde{f}(t) = \frac{2}{c}\left[f_t(t)v(t) + f_t'(t)R(t)\right]. \tag{15}$$

Equation (15) shows that the instantaneous frequency of the dechirp signal is composed of the frequency shift introduced by vibration velocity and the range displacement introduced by the nonlinearity, which causes great interference to the ranging results. Therefore, compensating for the coupling vibration error and nonlinear frequency modulation error is essential for improving the ranging accuracy of FMCW Lidar.

3. Time-Varying Vibration and Nonlinearity Compensation Method

To compensate for the vibration and nonlinearity for one-period T-FMCW Lidar, this section first extends the traditional ranging model to an instantaneous ranging model based on second-order SST which could depict the time-frequency characteristics of the dechirp signals. Then, the Lidar ranging system is introduced and the time-varying vibration and nonlinearity compensation method based on the PF model using the instantaneous ranges is derived. Finally, we summarize the workflow of the proposed method.

3.1. Instantaneous Ranging Model Based on Second-Order SST

This subsection will derive the instantaneous ranging model using the instantaneous frequencies of one-period FMCW dechirp signal. Second-order SST method is useful in characterizing the small perturbations of dechirp signals which contain severe time-varying vibration and nonlinearity errors. Thus, we obtain the instantaneous frequency using the second-order SST because of its high time-frequency resolution.

First, we apply the short-time Fourier transform (STFT) to a dechirp signal $\widetilde{s}_{if}(t')$ with coupling errors:

$$V^g(f_V, t) = \int_{-\infty}^{\infty} \widetilde{s}_{if}(t') g(t' - t) e^{-2i\pi f_V (t'-t)} dt', \tag{16}$$

where V^g and f_V are the time-frequency spectrum and the instantaneous frequency of the dechirp signal, respectively; and g is the gate function of STFT. The rearrangement operator of the first-order SST can be defined as [33]

$$\omega(f_V, t) = \frac{1}{2\pi}\partial_t \arg V^g(f_V, t) = f_V + Im\left(\frac{1}{2\pi}\frac{V^{g\prime}(f_V, t)}{V^g(f_V, t)}\right), \tag{17}$$

$$\tau_V(f_V, t) = t - \frac{1}{2\pi}\partial_{f_V} arg V^g(f_V, t) = t + Re\left(\frac{1}{2\pi}\frac{V^{tg}(f_V, t)}{V^g(f_V, t)}\right), \tag{18}$$

where ω is the approximation of the instantaneous frequency, and τ_V is the group delay.

Second, we calculate the second-order modulation operator and determine the rearrangement operator of second-order SST. The second derivative of the phase of STFT is defined as the modulation operator, which can be expressed as follows:

$$q(f_V, t) = Re\left\{\frac{\partial_t[\partial_t V^g(f_V, t)]/V^g(f_V, t)}{2i\pi - \partial_t\left[\partial_{f_V} V^g(f_V, t)\right]/V^g(f_V, t)}\right\}, \tag{19}$$

where $V^g(f_V, t) \neq 0$; and $\partial_t\left[\partial_{f_V} V^g(f_V, t)\right]/V^g(f_V, t) \neq 2i\pi$. $q(f_V, t)$ can be regarded as a measurement operator of the variation of energy rearrangement operator. The estimation operator of second-order instantaneous frequency is defined as

$$\hat{\omega}(f_V, t) = \begin{cases} \omega(f_V, t) + q(f_V, t)(t - \tau_V(f_V, t)) & if \quad \partial_t \tau_V(f_V, t) \neq 0 \\ \omega(f_V, t) & otherwise \end{cases}. \tag{20}$$

Third, we rearrange the time-frequency spectrum by using the second-order instantaneous frequency, and (f_V, t) is transformed to $[\omega(f_V, t), t]$. Thus, the time-frequency spectrum of STFT is accumulated to the second-order frequency obtained by using Equation (20), and the second-order SST can be expressed as follows:

$$T_V = \frac{1}{g(0)}\int_{-\infty}^{\infty} V(f_V, t)\delta[\omega - \hat{\omega}(f_V, t)] df_V, \tag{21}$$

where T_V is the second-order synchrosqueezing result. The energy of the instantaneous frequency is squeezed to the central frequency by using Equation (21), which obtains time-frequency curves with higher resolution. Due to the localization of the estimation operators, second-order SST can depict small perturbations of the dechirp signals which is effective in dealing with severe time-varying vibration and nonlinearity errors [34].

Fourth, we can extract the instantaneous frequency curve $\widetilde{f}$ as shown in Equation (15) from the squeezing result by using the ridge detection method.

At last, we can obtain the instantaneous range of the dechirp signal:

$$\begin{aligned} \widetilde{R}(t) &= \frac{\widetilde{f}(t)c}{2K} = \frac{1}{K}[f_t(t)v(t) + f_t'(t)R(t)] \\ &= \frac{1}{K}[f_c + Kt + f_e(t)]v(t) + \frac{1}{K}[K + f_e'(t)]R(t) \quad , \\ &\approx R_0(t) + \frac{f_c}{K}[v_0(t) + v_e(t)] + \frac{f_e'(t)}{K}R_0(t) \\ &= R_0(t) + \frac{f_c}{\Delta f_c}\Delta\varepsilon_{v0}(t) + \frac{f_c}{\Delta f_c}\Delta\varepsilon_{ve}(t) + \frac{f_e'(t)}{K}R_0(t) \end{aligned} \tag{22}$$

where $R_0(t)$ represents the actual range of target relative to fiber range; $v(t) = v_0(t) + v_e(t)$ is the velocity of vibration; $v_0(t)$ is the steady-state velocity; $v_e(t)$ is the disturbance velocity;

$\Delta\varepsilon_{v0}(t)$ is the steady-state error induced by $v_0(t)$; $\Delta\varepsilon_{ve}(t)$ is the disturbance error induced by $v_e(t)$; and Δf_c is the frequency scan scope. In Equation (22), $[t + f_e(t)/K]v(t)$ is ignored because it is on the order of micrometer, while $R(t)$ is approximated by $R_0(t)$ because the vibration in $R(t)$ is not amplified and is small compared with the range of target.

Equation (22) is the instantaneous ranging model which takes advantage of the localized characteristics of the dechirp signal in time-frequency domain to extend the traditional range into the instantaneous range. We should note that Equation (22) is derived for an up dechirp signal, and the plus sign should be replaced by the minus sign when the input data is a down dechirp signal. From the above Equation, we can see that the instantaneous range contains two parts of errors, namely vibration error introduced by the Doppler Effect (including steady-state error and time-varying disturbance error), and the nonlinearity error introduced by nonlinear frequency modulation of the Lidar system. The vibration error is amplified by factor $f_c/\Delta f_c$, and the nonlinearity error is amplified by the nonlinearity factor $f_e'(t)/K$. Thus, the coupling errors will seriously affect the ranging accuracy, and it is essential to compensate for the time-varying vibration error coupled with the nonlinearity error.

We define $\eta = f_c/\Delta f_c$ and $\xi(t) = f_e'(t)/K$, then Equation (22) can be rewritten as follows

$$\widetilde{R}(t) = R_0(t) + \eta\Delta\varepsilon_{v0}(t) + \eta\Delta\varepsilon_{ve}(t) + \xi(t)R_0(t). \tag{23}$$

To show the advantages of second-order SST over STFT and first-order SST, we simulated a multi-component signal containing two modes, namely Mode 1 and Mode 2. The equations for Mode 1 and Mode 2 are $\sin\{2\pi[300t + 16\cos(3\pi t)]\}$ and $\exp\left[-8(t-0.5)^2\right]\sin(100\pi t)$, respectively, and the time-domain diagrams of the modes are shown in Figure 3a. STFT was first used to transform two modes to the time-frequency domain, and the result is shown in Figure 3b. STFT can generally reflect the time-frequency distribution of two modes, but the energy of the effective signal is diffuse. Then we applied first-order SST and second-order SST to the modes in Figure 3a, and the time-frequency distributions of two modes are shown in Figure 3c,d, respectively. Both the first-order SST and second-order SST methods can effectively compress the energy of useful signals in time-frequency domain compared with the STFT result. As shown in Figure 3c,d, the energy of single-frequency signal Mode 2 in the first-order SST and second-order SST results are similar. However, one limitation of the first-order SST is that it assumes the effective signal is weakly modulated [35]. Thus, the energy of strongly modulated signal Mode 1 in the second-order SST result is more focused and sharper than that in the first-order SST. In a T-FMCW Lidar system, the dechirp signals may be strongly modulated because of the time-varying coupling errors, and therefore the second-order SST method is more suitable for depicting the time-frequency distribution of the dechirp signals.

In order to compare the first-order SST with the second-order SST in dealing with noisy signals, we added Gaussian white noise with a signal-to-noise ratio (SNR) of 5 dB to the signal, and the time-frequency distributions of two modes after the first-order SST and the second-order SST are shown in Figure 3e,f, respectively. Figure 3e,f shows that noise increases the difficulty of signal recognition in time-frequency domain and the first- and second-order SST results of Mode 2 with noise are similar. However, the second-order SST result of Mode 1 is more continuous and clearer than the first-order SST result, as the second-order SST has better time-frequency concentration for strongly modulated signals. Thus, the second-order SST performs better than the first-order SST in the presence of noise.

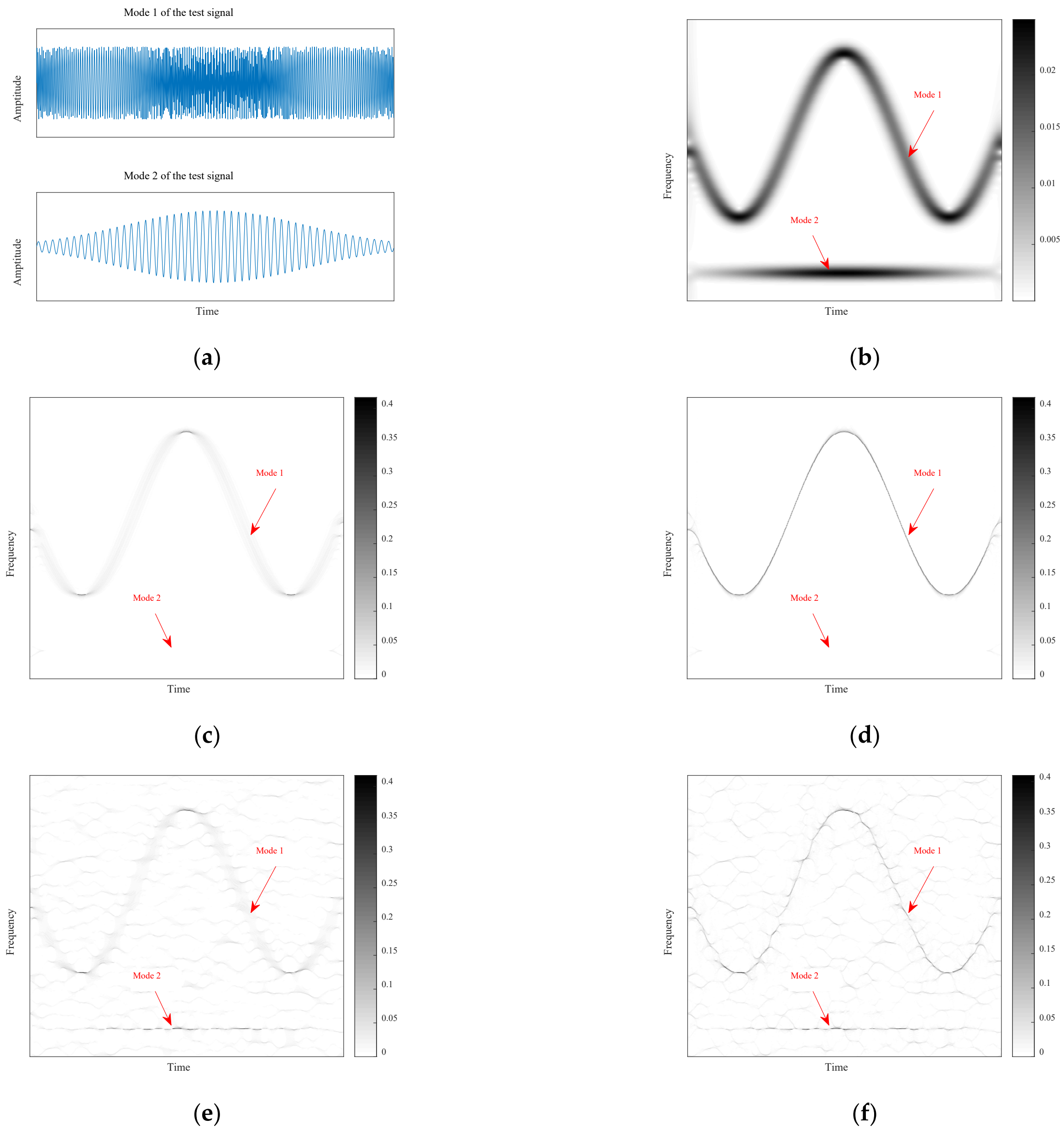

Figure 3. Comparison of short-time Fourier transform (STFT), first-order synchro-squeezing transform (SST) and second-order SST: (**a**) time-domain diagrams of the test signal which contains two modes; STFT result (**b**), first-order SST result (**c**) and second-order SST result (**d**) of the clean signal; first-order SST result (**e**) and second-order SST result (**f**) of the noisy signal with SNR of 5 dB.

3.2. Lidar System Design and Time-Varying Vibration and Nonlinearity Compensation Method

Figure 4 shows the schematic diagram of a FMCW Lidar system which includes a measurement channel and an auxiliary channel. The laser source is generated by two steps. We first generate a single-frequency laser signal and a microwave frequency modulation signal. Then we apply a Mach–Zehnder modulator to the laser signal by using the driven signal and obtain the FMCW laser source [3]. The tunable laser source is divided into two beams by coupler 1 as the local oscillator signals of the measurement channel and the auxiliary channel, respectively. The oscillator signal in the measurement channel is divided into two laser beams through coupler 2. One of the local oscillator signals is transmitted by an optical antenna and reflected to the antenna when encountered a target. The other beam separated by coupler 2 passes through a delay fiber and then divided into two laser beams through coupler 3. One beam separated by coupler 3 interferes with the received signal through coupler 4, then the dechirp signal is coherently acquired by the measurement detector D_{MAIN}. The oscillator signal in the auxiliary channel separated by coupler 1 passes through a delay fiber and then interferes with the other beam of coupler 3 through coupler 5. Then the dechirp signal of the auxiliary channel is coherently acquired by the auxiliary detector D_{AUX} [22]. The dechirp signals obtained from the auxiliary channel and the measurement channel are simultaneously sampled by digital acquisition card DAQ, and then the data are imported into the computer for subsequent signal processing.

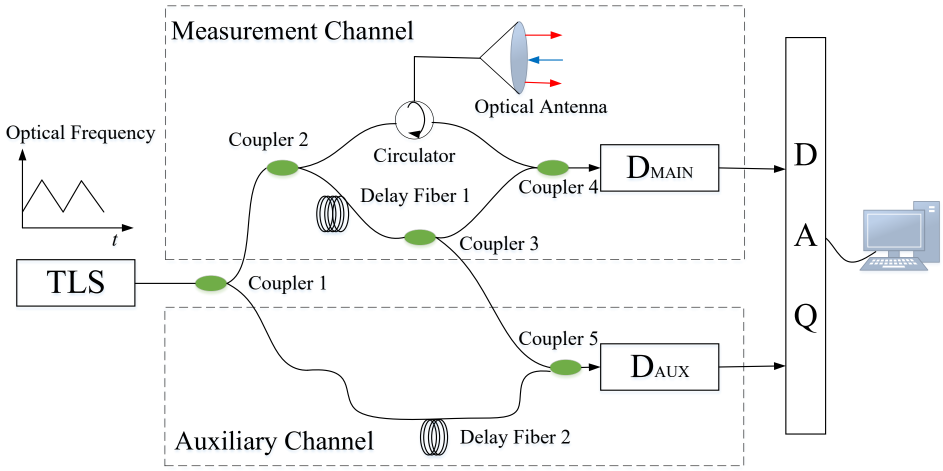

Figure 4. Schematic diagram of frequency modulation continuous wave (FMCW) coherent Lidar System. TLS: tunable laser source; D_{MAIN}: measurement detector; D_{AUX}: auxiliary detector; DAQ: data acquisition card.

As shown in Figure 4, the local oscillator signal is delayed by delay fiber 1 and then mixed with the reflected signal in the measurement channel. The introduction of a delay fiber can reduce the requirement for high-coherence of the laser source and thereby improve the detection range [36]. The dechirp signals obtained from the auxiliary channel and the measurement channel will be referred to as the reference dechirp signal and the measurement dechirp signal, respectively, in the following part.

The general idea of the time-varying vibration and nonlinearity compensation method is as follows. First, the instantaneous ranges of the reference dehirp signal and the measurement dechirp signal are obtained according to the instantaneous ranging model based on the second-order SST, and the nonlinearity error of the system is estimated by using the time-frequency information of the auxiliary channel. The ranges of the auxiliary channel and measurement channel will be referred to as the reference range and the measurement range, respectively. Then, we preliminarily compensate for the nonlinearity error in the instantaneous measurement range by using the estimated nonlinearity error of the auxiliary channel. The basic principle of our method, which uses an auxiliary channel to compensate for the nonlinearity error, is similar to [18–20]. However, when the nonlinearity error cannot be estimated accurately, the residual nonlinearity error will degrade the final ranging results. To solve this problem, we build the PF model to compensate for the residual nonlinearity error and the time-varying vibration error, and the actual range of target is tracked accurately by using the triangular symmetry relations of the up and down observation of T-FMCW. In the following part, the dechirp signals of up and down observations of T-FMCW will be referred to as the up dechirp signal and down dechirp signal. Correspondingly, the ranges obtained from the up dechirp signal and down dechirp signal will be referred to as the up range and down range, respectively.

The up observation of T-FMCW is taken as an example for deriving the time-varying vibration error and nonlinearity error compensation process. First, the instantaneous reference range $\widetilde{R}_{ref}(t)$ is obtained by substituting the reference dechirp signal into the instantaneous ranging model:

$$\widetilde{R}_{ref}(t) = \frac{F_{ref}(t)c}{2K} = R_{ref0}(t) + \xi(t)R_{ref0}(t), \tag{24}$$

where $F_{ref}(t)$ is the center frequency curve of the reference dechirp signal obtained using second-order SST; and $R_{ref0}(t)$ is the actual range of the auxiliary channel. The nonlinearity factor $\hat{\xi}(t)$ of the Lidar system can be estimated by using the following Equation:

$$\hat{\xi}(t) = \frac{\widetilde{R}_{ref}(t) - R_{ref0}(t)}{R_{ref0}(t)}. \tag{25}$$

Then, the instantaneous measurement range $\widetilde{R}_m(t)$ can be calculated by substituting the measurement dechirp signal to Equation (23), which is expressed as follows:

$$\widetilde{R}_m(t) = \frac{F_m(t)c}{2K} = R_{m0}(t) + \eta\Delta\varepsilon_{v0}(t) + \eta\Delta\varepsilon_{ve}(t) + \hat{\xi}(t)R_{m0}(t). \tag{26}$$

where $F_m(t)$ is the center frequency curve of the measurement dechirp signal obtained using second-order SST; and $R_{m0}(t)$ is the actual range of target. Since the range of the delay fiber in auxiliary channel is close to the detection range of Lidar system, the nonlinearity error $\hat{\xi}(t)R_{ref0}(t)$ in the auxiliary channel can be used to compensate for the nonlinearity error $\hat{\xi}(t)R_{m0}(t)$ in the measurement channel. The instantaneous up and down measurement ranges $\widetilde{R}_{up}(t)$ and $\widetilde{R}_{down}(t)$ after preliminarily compensating for the nonlinearity error can be expressed as

$$\begin{cases} \widetilde{R}_{up}(t) = R_{m0}(t) + \frac{f_c}{\Delta f_c}\Delta\varepsilon_{v0}(t) + \frac{f_c}{\Delta f_c}\Delta\varepsilon_{ve1}(t) + \Delta\varepsilon_{non1}(t) \\ \widetilde{R}_{down}(t) = R_{m0}(t) - \frac{f_c}{\Delta f_c}\Delta\varepsilon_{v0}(t) - \frac{f_c}{\Delta f_c}\Delta\varepsilon_{ve2}(t) + \Delta\varepsilon_{non2}(t) \end{cases}, \tag{27}$$

where $\Delta\varepsilon_{non1}(t)$ and $\Delta\varepsilon_{non2}(t)$ are the residual nonlinearity error of up and down observations; $\Delta\varepsilon_{ve1}(t)$ and $\Delta\varepsilon_{ve2}(t)$ are disturbance errors in the up and down observations. We assume that the steady-state vibration velocities of up and down observation are equal due to the short frequency sweep period, which means the steady-state error $\Delta\varepsilon_{v0}(t)$ in the up observation equals to that in the down observation. If the disturbance errors $\Delta\varepsilon_{ve1}(t)$ and $\Delta\varepsilon_{ve2}(t)$ in the up and down observation are equal and the residual nonlinearity errors $\Delta\varepsilon_{non1}(t)$ and $\Delta\varepsilon_{non2}(t)$ can be negligible too, we can compensate for the vibration error and estimate the target range by adding half of the up range and half of the down range $R_{m0} = \left(\widetilde{R}_{up} + \widetilde{R}_{down}\right)/2$. However, the disturbance error in the up observation is different from that in the down observation when the vibration is severe because there is half-period time delay between the two observations, and there will be an estimation error if we estimate the target range by directly adding half of the up range and half of the down range. Therefore, we construct a PF model using the instantaneous range for the T-FMCW Lidar signal, by which we can filter out the disturbance errors and the residual nonlinearity errors from the up and down measurement ranges. Then the filtered ranges only contain steady-state errors, and the target range can be estimated by adding half of the up range and half of the down range.

For a Lidar working in the vibration environment, the instantaneous measurement range can be expressed by second-order Taylor expansion when the sampling interval Δt is very small

$$R_{k+1} = R_k + v_k\Delta t + \frac{1}{2}a_k\Delta t^2, \tag{28}$$

where R_{k+1} and R_k represent the $(k+1)$th and kth instantaneous ranges; Δt is the sampling interval; v_k and a_k denote the first and second derivatives of R_k, respectively. Equation (28) is the state function of FMCW Lidar observation system.

By combining Equation (27) with Equation (28), we obtain the measurement function

$$\widetilde{R}_k = R_k + \eta_k v_k \Delta t + \frac{1}{2}\eta_k a_k \Delta t^2 + \Delta\varepsilon_{nonk}, \tag{29}$$

where $\widetilde{R}_k$ and R_k represent the measurement range and the filtered range, respectively; $\eta_k = \pm f_c/\Delta f_c$ represents amplification factor; and the sign of η_k is positive for up-dechirp signal and negative for down-dechirp signal; and $\Delta\varepsilon_{nonk}$ represents the residual nonlinearity error at the kth moment. Equation (29) is the measurement function of the FMCW Lidar observation system.

Then, we build a PF model for T-FMCW to obtain the filtered ranges of the instantaneous measurement range. Assuming that the state vector of PF is $\mathbf{x}_k = [R_k \ \ v_k \ \ a_k]^T$, then the state vector at the $(k+1)$th moment can be expressed as

$$\mathbf{x}_{k+1} = \begin{bmatrix} 1 & \Delta t & \Delta t^2/2 \\ 0 & 1 & \Delta t \\ 0 & 0 & 1 \end{bmatrix} \mathbf{x}_k + \boldsymbol{\alpha}_k, \tag{30}$$

where $\boldsymbol{\alpha}_k$ represents the noise vector that obeys Gaussian distribution. The measurement vector is expressed as

$$\mathbf{y}_k = \begin{bmatrix} 1 & \eta_k \Delta t & \frac{\eta_k \Delta t^2}{2} \end{bmatrix} \mathbf{x}_k + \boldsymbol{\beta}_k, \tag{31}$$

where $\boldsymbol{\beta}_k$ is the measurement noise containing residual nonlinearity error. The up filtered range R_{up} and down filtered range R_{down} can be obtained by applying PF to the instantaneous ranges of Equation (31). The filtered range of target after PF tends to be a steady-state value that is close to the true state, and the corresponding time of the steady-state value can be regarded as the evaluation time. Thus, the time-varying disturbance error and residual nonlinearity error can be eliminated. The workflow of PF can be found in [24], and we do not discuss it here.

Finally, we estimate the range of the target by using the filtered ranges. The filtered ranges R_{up} and R_{down} of up and down observation can be expressed as

$$R_{up} = R_{m0} + \frac{f_c}{\Delta f_c}\Delta\varepsilon_{v0}, \tag{32}$$

$$R_{down} = R_{m0} - \frac{f_c}{\Delta f_c}\Delta\varepsilon_{v0}. \tag{33}$$

By combining Equation (32) with Equation (33), we can obtain the measurement range R_{m0}

$$R_{m0} = \frac{R_{up} + R_{down}}{2}. \tag{34}$$

Thus, the time-varying vibration error coupled with nonlinearity error can be eliminated by using the PF method for T-FMCW, and the actual range of the target can be estimated accurately.

3.3. Workflow of the Proposed Method

The workflow of the simultaneous time-varying vibration and nonlinearity compensation method for one-period T-FMCW Lidar is summarized as follows.

(a): Extract up and down dechirp signals from one-period T-FMCW Lidar signals. The up and down measurement dechirp signals obtained from the measurement channel are denoted as $s_{m1}(t)$ and $s_{m2}(t)$, respectively. The up and down reference dechirp signals obtained from the auxiliary channel are denoted as $s_{ref1}(t)$ and $s_{ref2}(t)$, respectively.

(b): Calculate the second-order modulation operators and the estimation operator of second-order instantaneous frequency for reference dechirp signals and measurement dechirp signals by using Equations (19) and (20), and determine the criterion of energy rearrangement.
(c): Rearrange the time-varying spectrums by using the second-order estimation operator and obtain the squeezing results by using Equation (21).
(d): Extract central time-frequency curves based on the ridge detection method. The time-frequency curves of the up and down measurement dechirp signals are denoted as $F_{m1}(t)$ and$F_{m2}(t)$, respectively. The time-frequency curves of the up and down reference dechirp signals are denoted as $F_{ref1}(t)$ and $F_{ref2}(t)$, respectively.
(e): Calculate the instantaneous measurement ranges $\widetilde{R}_{m1}(t)$ and $\widetilde{R}_{m2}(t)$ corresponding to $F_{m1}(t)$ and $F_{m2}(t)$, and the instantaneous reference ranges $\widetilde{R}_{ref1}(t)$ and $\widetilde{R}_{ref2}(t)$ corresponding to $F_{ref1}(t)$ and $F_{ref2}(t)$ by using Equation (23).
(f): Estimate the nonlinearity errors $\hat{\xi}_1(t)$ and $\hat{\xi}_2(t)$ of up and down observations by using $\widetilde{R}_{ref1}(t)$ and $\widetilde{R}_{ref2}(t)$ according to Equation (25), and eliminate $\hat{\xi}_1(t)$ and $\hat{\xi}_2(t)$ from the instantaneous measurement ranges $\widetilde{R}_{m1}(t)$ and$\widetilde{R}_{m2}(t)$. The instantaneous ranges after preliminarily compensating for the nonlinearity errors are denoted as $\widetilde{R}_{up}(t)$ and $\widetilde{R}_{down}(t)$.
(g): Construct the state function and measurement function of $\widetilde{R}_{up}(t)$ and $\widetilde{R}_{down}(t)$ using Equations (28) and (29).
(h): Establish the PF model for T-FMCW, and compensate for the disturbance errors and the residual nonlinearity errors by applying PF to $\widetilde{R}_{up}(t)$ and $\widetilde{R}_{down}(t)$.
(i): Substitute the filtered ranges into Equation (34) to estimate the actual range of target.

4. Experimental Analysis

We used four experiments to prove the validity of the proposed method. The first two experiments are one-dimensional ranging verifications, in which the first experiment adds only nonlinearity error to the ideal dechirp signal, and the second experiment adds time-varying vibration error coupled with nonlinearity error to the ideal dechirp signal. The third experiment compares the ranging performance of the proposed method and the three-point method proposed in [12] in dealing with severe vibration. The last experiment is used to verify the applicability of the proposed method in 3D imaging. The parameters of FMCW Lidar are shown in Table 1.

Table 1. Parameters of frequency modulation continuous wave (FMCW) Lidar.

Parameters	Values
Waveform	T-FMCW
Period	4 ms
Wavelength of laser	1.55 μm
Bandwidth	1 GHz

4.1. Prove the Validity of the Proposed Method with Nonlinearity

The first example added a sinusoidal error to the ideal frequency modulation rate, and the error is shown as $4.5 \times 10^9 \times \sin(2\pi \times 1600t)$. The range of target is 1525 m and the reference range of auxiliary channel is 1523 m. Figure 5a shows the up and down measurement dechirp signals with nonlinearity errors. For contrast, the ideal measurement dechirp signal is also shown in Figure 5a with dashed lines. Then, Fourier transform was applied to the dechirp signals in Figure 5a to obtain frequency spectrums and the range distributions of target, and the range profile is shown in Figure 5b. Due to the influence of nonlinearity error, the dechirp signals in Figure 5a are distorted compared with the ideal dechirp signal. Figure 5b shows that the nonlinearity error leads to the rising of side lobe and the decrease of resolution in one-dimensional range profiles, which degrades the accuracy of subsequent imaging results.

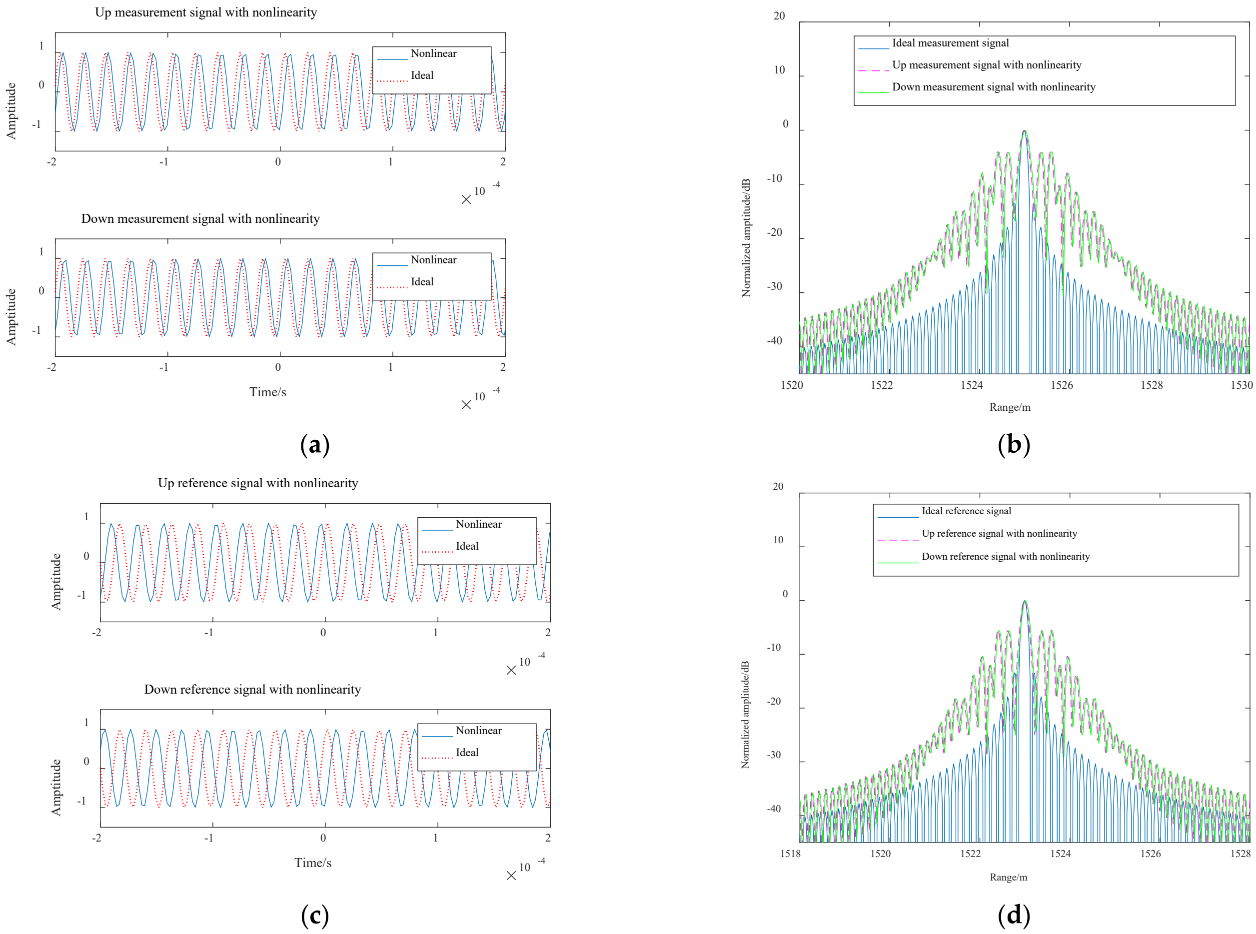

Figure 5. (**a**) Up and down measurement dechirp signals with nonlinearity error; (**b**) One−dimensional range profiles of the measurement dechirp signals; (**c**) Up and down reference dechirp signals with nonlinearity error; (**d**) One−dimensional range profiles of the reference dechirp signals.

The fiber range can be designed according to the range of the actual detection target. In our experiments, the target range was 1525 m and the range of delay fiber 1 shown in Figure 4 was set to be 1510 m after taking account of the refractive index. Thus, the frequency was calculated to be approximately 50 kHz by using the measurement dechirp signal that was obtained by coherent detection (coherently mixing the reflected signal and the delayed local oscillator signal). The time-domain diagrams and one-dimensional range profiles of the up and down reference dechirp signals are shown in Figure 5c,d, and the dashed lines represent the ideal reference dechirp signal. Figure 5c,d shows that the time-domain curves of the reference dechirp signals are also distorted due to the nonlinearity error, and the range profiles have broadened main lobe and uplifted side lobe, which is similar to Figure 5a,b.

The proposed method was then used to estimate the range of target. First, the measurement dechirp signals and the reference dechirp signals with the nonlinearity error as shown in Figure 5 were transformed into time-frequency domain by using the second-order SST, and the results are shown in Figure 6. Figure 6a shows the time-frequency curves of up measurement and up reference dechirp signals, while Figure 6b shows the time-frequency curves of down measurement and down reference dechirp signals. The second-order SST result of the ideal reference dechirp signal is shown in Figure 7a for comparison. Figures 6 and 7a show that the dechirp signal is a single-frequency signal in the ideal case and the time-frequency curve with nonlinearity error is a superposition of nonlinearity term and ideal single-frequency curve. Thus, the time-frequency curve bends considerably, which leads to the distortion of one-dimensional range profiles as shown in Figures 4b and 5b. In addition, since the transmitted signals with nonlinear frequency errors of Lidar system occur simultaneously in the auxiliary channel and the measurement channel, the distortion of time-frequency curves of the reference and the measurement dechirp signals in Figure 6 are consistent.

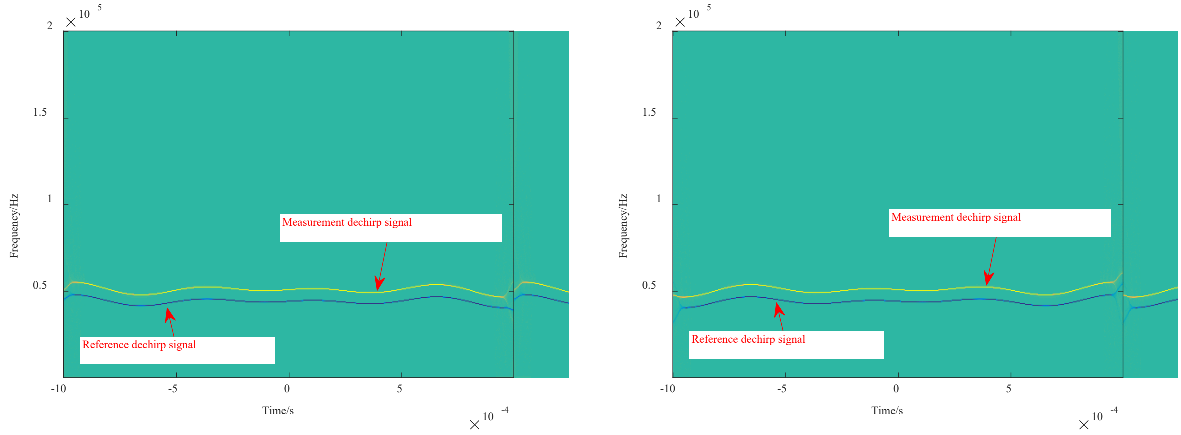

(**a**) (**b**)

Figure 6. (**a**) The second−order SST results of up measurement and up reference dechirp signals; (**b**) The second−order SST results of down measurement and down reference dechirp signals.

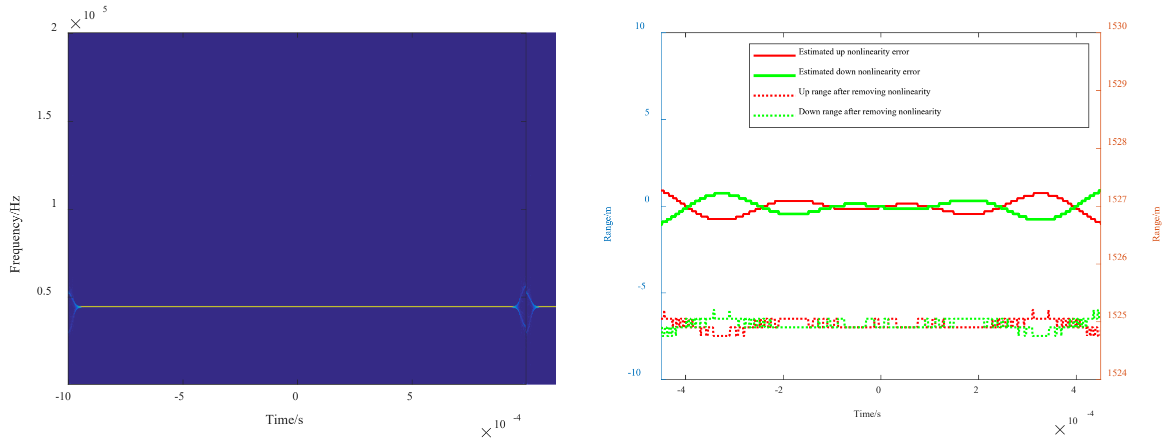

(**a**) (**b**)

Figure 7. (**a**) The second−order SST results of ideal reference dechirp signal; (**b**) The estimated nonlinearity errors (shown by the left axis) and the preliminarily compensation results of the instantaneous measurement ranges (shown by the right axis).

The ridge detection method was used to track the center time-frequency curves of the reference and the measurement dechirp signals in Figures 6 and 7a, respectively, and the instantaneous measurement and reference ranges were obtained according to the instantaneous ranging model, as shown in Equation (23). Combined with Equation (25), the time-frequency information of the auxiliary channel is used to estimate the nonlinearity error of the dechirp signals, and the results are shown in Figure 7b by the left axis.

Then, we used Equation (27) to preliminarily compensate for the nonlinearity errors in the up and down instantaneous measurement ranges, respectively, and the compensated results are shown in Figure 7b by the right axis. Finally, we used the PF model for T-FMCW to filter out the interference noise including residual nonlinearity error from the instantaneous measurement range in Figure 7b, and the range of target can be calculated according to the triangular symmetry relations as shown in Equations (32) and (33). The up and down filtered ranges and the estimated range are shown in Figure 8a, in which the estimated range of target tends to be a steady-state value and the corresponding evaluation time is 900 μs. The steady-state value (1525.05 m) is regard as the final estimated range of target which is close to the actual range (1525 m), indicating that the proposed method can effectively eliminate the nonlinearity error and accurately estimate the range of target.

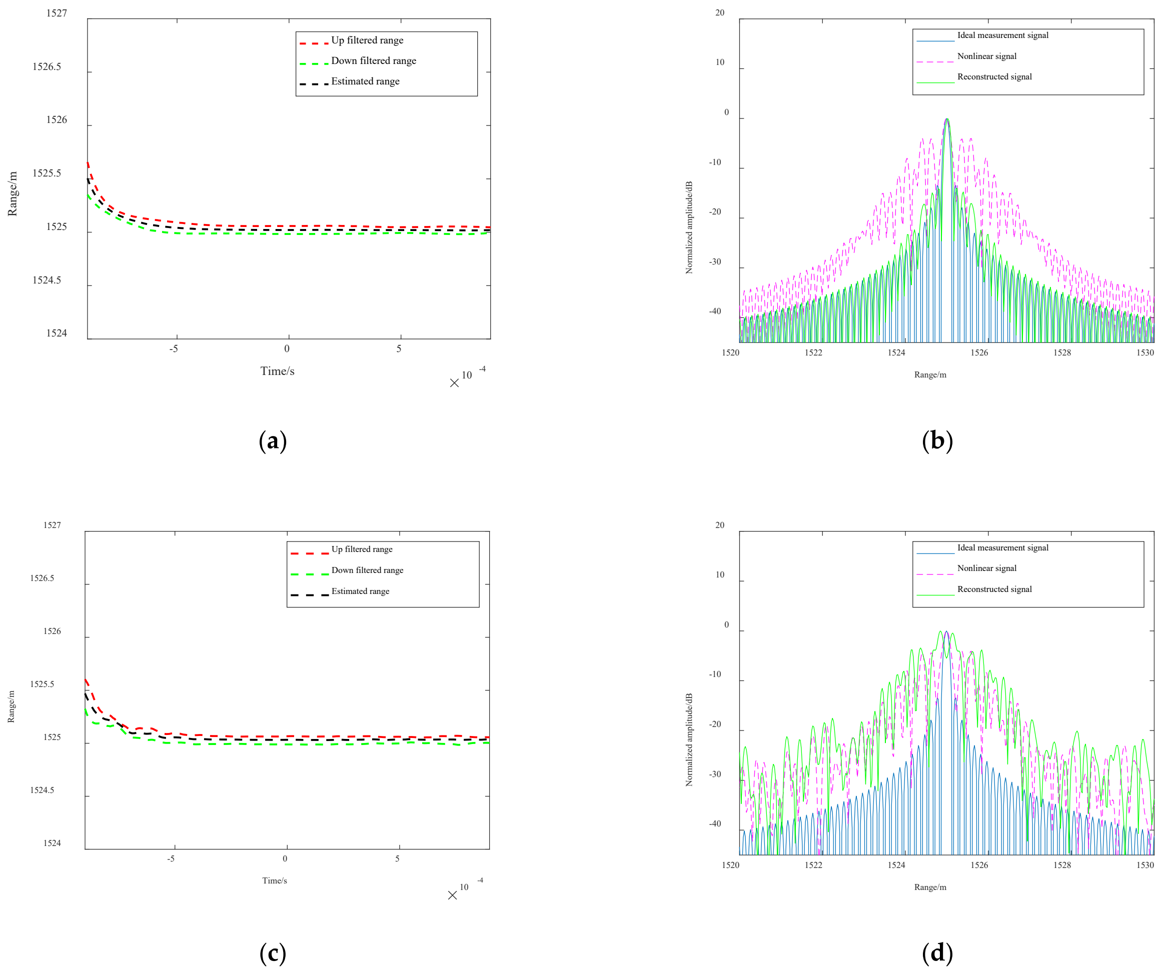

Figure 8. The estimated ranges of the proposed method (**a**) and the envelope detection method (**b**); the estimated ranges of the proposed method (**c**) and the envelope detection method (**d**) in the noisy environment with SNR of 5 dB.

We also conducted an experiment to make a comparison between the envelope detection method [20] and the proposed method. Figure 8b shows the estimated range of the envelope detection method. We should note that the proposed method extends the ranging model to an instantaneous ranging model so that the ranges in Figure 8a are time-varying, and the range profile of the envelope detection method is independent of time. The range profile of the envelope detection method is also close to the ideal range profile and the estimated range is 1525.05 m, as shown in Figure 8b. We then added Gaussian white noise with a signal-to-noise ratio (SNR) of 5 dB into the transmitted signal. Figure 8c,d shows the estimated ranges of the proposed method and the envelope detection method from noisy signals. The noise does not have obvious influence on the estimated ranges of the proposed method as the second-order SST and the Particle filter are robust to noise. However, the envelope detection method loses validity for noisy signals. The envelope detection method estimates the nonlinear frequency by detecting the amplitude envelope which is not robust to noise. As shown in Figure 8d, the spectrum energy of the range profile after nonlinearity compensation is still diffuse, which affects the recognition the final range. Therefore, the proposed method is more robust than the envelope detection method to noise.

4.2. Prove the Validity of the Proposed Method with Coupling Error

The second example added two sinusoidal vibration errors with frequencies of 900 Hz and 40 Hz and amplitudes of 2 µm and 50 µm which are coupled with the nonlinearity error shown in the above subsection, and Gaussian white noise with a signal-to-noise ratio (SNR) of 5 dB was also added to the measurement dechirp signal. The target range of this section is 1525 m, and the reference range of auxiliary channel is 1523 m. Figure 9a shows the up and down measurement dechirp signals with coupling errors, and the dashed lines represent the ideal measurement dechirp signals. Figure 9b shows the noisy measurement dechirp signals with SNR of 5 dB and coupling errors. The time-domain signals shown in Figure 9a are greatly distorted compared with the ideal dechirp signal due to the existence of time-varying vibration and nonlinearity errors, and the noise induces additional jitter to the curves as shown in Figure 9b. Fourier transform was then applied to the dechirp signals, and the frequency spectrums were converted to range profiles, as shown in Figure 9c,d. Time-varying coupling errors induce a big offset to the range of target in the one-dimensional range profiles shown in Figure 9c, and noise aggravates the difficulty of target recognition as shown in Figure 9d. Thus, regarding the peak of the range profiles as the range of target will seriously reduce the accuracy of target recognition and imaging.

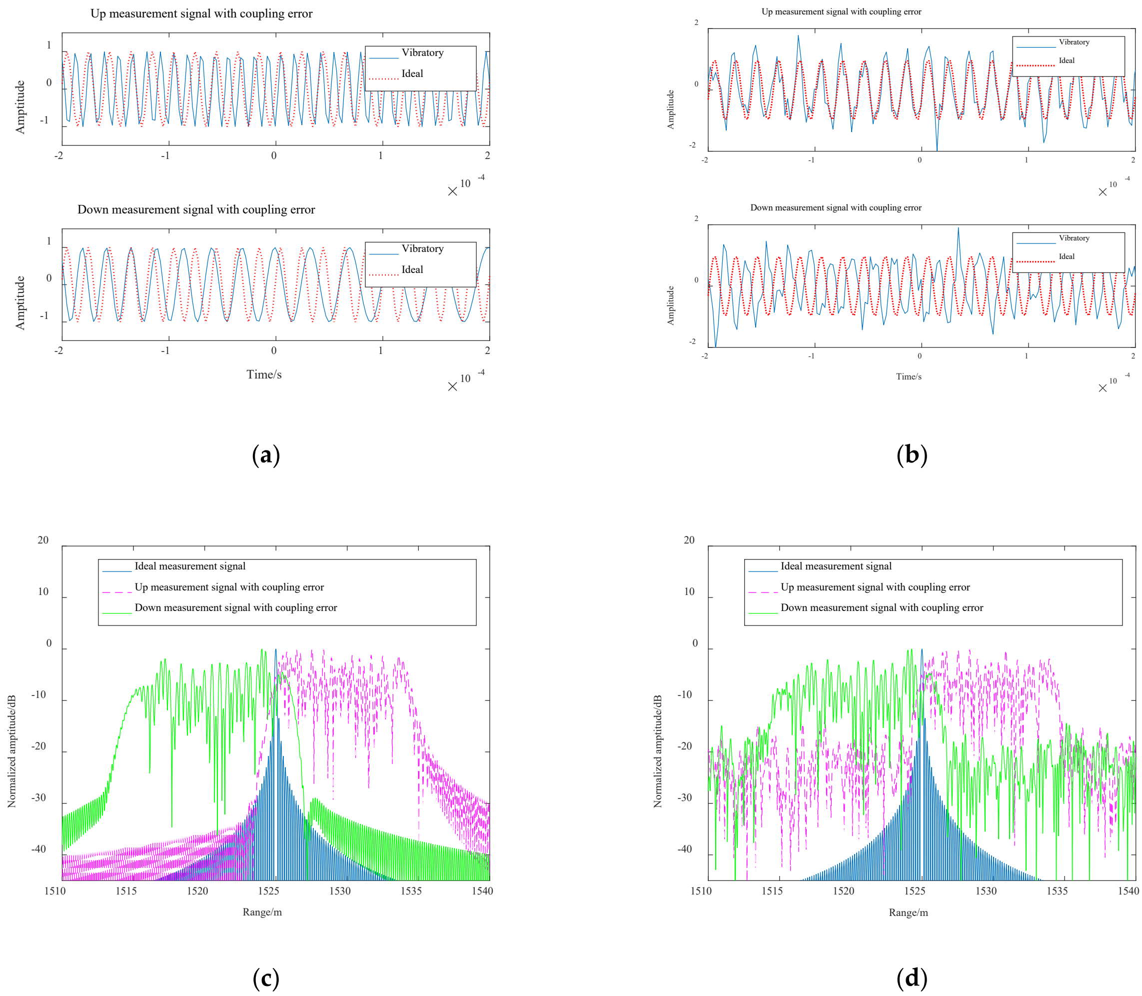

Figure 9. (**a**) Up and down measurement dechirp signals with coupling error; (**b**) Up and down measurement dechirp signals with coupling error and signal−to−noise ratio (SNR) of 5 dB; (**c**) One-dimensional range profiles of the measurement dechirp signals with coupling error; (**d**) One-dimensional range profiles of the measurement dechirp signals with coupling error and SNR of 5 dB.

The proposed time-varying vibration and nonlinearity compensation method was applied to the noisy dechirp signals shown in Figure 9b. Figure 10a shows the noisy reference dechirp signals with the nonlinearity error and SNR of 10 dB. The noise in reference dechirp signals is less than that in measurement dechirp signals, since the signals transmitted in the air suffer more interference than in the fiber. First, second-order SST was applied to the up and down reference dechirp signals shown in Figure 10a and the up and down measurement dechirp signals shown in Figure 9b. The time-frequency distributions of up and down reference dechirp signals are shown in Figure 10b and the time-frequency distributions of up and down measurement dechirp signals are shown in Figure 10c,d, respectively. Figure 10 verifies that the second-order SST results have high time-frequency resolution and can accurately depict the time-frequency distributions of effective signals. In addition, the time-frequency curves with coupling errors are seriously deviated from the ideal single-frequency signal. The noise in Figure 10c,d is squeezed and aggregated in the time-frequency domain, which makes the time-frequency distributions of the effective signals clearer.

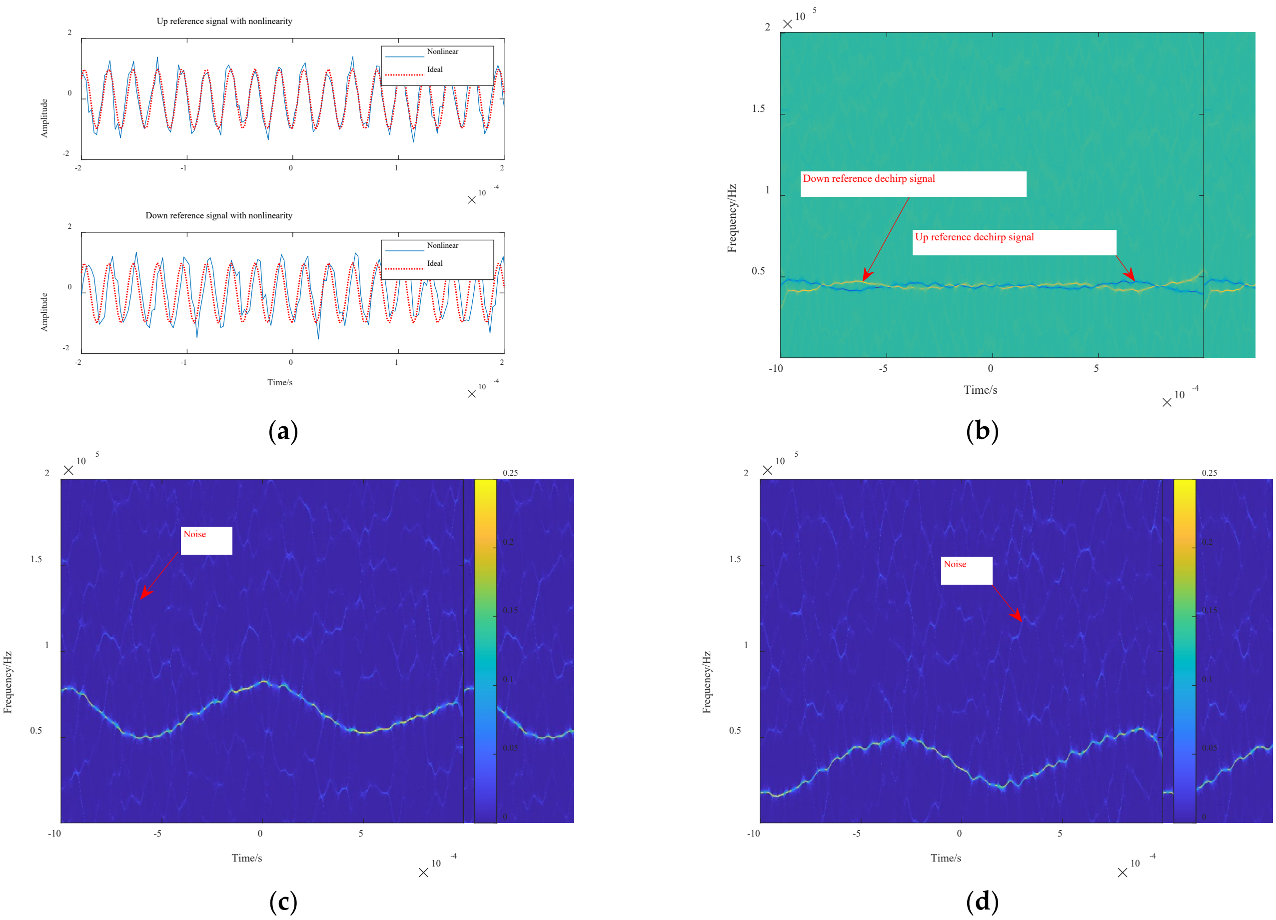

Figure 10. (**a**) Up and down reference dechirp signals with nonlinearity error and SNR of 10dB; (**b**) The second−order SST results of up and down reference dechirp signals; The second−order SST results of up measurement dechirp signal; (**c**) and down measurement dechirp signal (**d**).

Then, the center time-frequency curves of the measurement dechirp signals and the reference dechirp signals shown in Figure 10b–d were tracked by the ridge detection method, and the instantaneous reference ranges and the measurement ranges are obtained according to Equation (23). The time delay information of the reference dechirp signal was used to estimate the nonlinearity error, as shown in Figure 11a by the left axis, and the instantaneous up and down ranges after preliminarily compensating for the nonlinearity error are shown in Figure 11a by the right axis. Finally, the PF model for T-FMCW was established to filter out the residual nonlinearity error and other interference noise from the instantaneous up and down ranges. Additionally, the range of target can be calculated according to the triangular symmetry relations in Equations (32) and (33). The up and down filtered ranges and the estimated range are shown in Figure 11b. The evaluation time of Figure 11 is 900 µs and the final range of target was estimated to be 1524.95 m, which is close to the ideal range of target (1525 m).

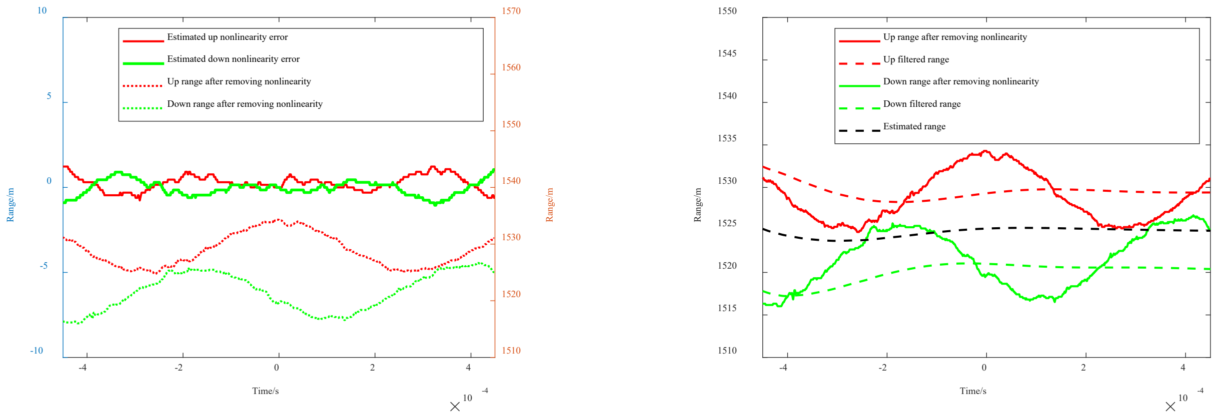

(**a**) (**b**)

Figure 11. (**a**) The estimated nonlinearity errors (shown by the left axis) and the preliminarily compensation results of the instantaneous measurement ranges (shown by the right axis); (**b**) The filtered ranges and the estimated range of target.

4.3. Compare the Ranging Performance with Traditional Three-Point Method

Since the traditional three-point method proposed by [12] could compensate for vibration by using only one-period signals without additional lasers, we compare this method with the proposed method in this subsection. However, the three-point method does not compensate for the nonlinearity error. Thus, we applied the three-point method to the dechirp signals with only vibration error, while we applied the proposed method to the dechirp signals with both the vibration error and nonlinearity error. We added two sinusoidal vibration errors with frequencies of 900 Hz and 40 Hz and Gaussian white noise with SNR of 0 dB to the measurement dechirp signal. The target range of this subsection is 1525 m, and the reference range of auxiliary channel is 1523 m. We first applied the three-point method to the dechirp signals with severe vibration, and the phases with vibration are shown in Figure 12a. Here, we also drew the phases of ideal dechirp signals for comparison, and the result is shown in Figure 12b. In Figure 12, the blue lines and red lines represent the up and down observations, respectively. Compared with the phases in Figure 12b, the phases in Figure 12a are distorted due to the severe vibration and noise. The range of target was estimated to be 1523.56 m by using the calculated phases of the three-point method. Then, we added nonlinearity error as shown in subSection 4.2 to the dichirp signals with severe vibration and noise, and applied the proposed method to the dechirp signals with both vibration and nonlinearity errors. The range of target was estimated to be 1525.09 m which is closer to the ideal range.

Root mean square error (RMSE) is an important indicator to reflect a statistical result of range measurement [37]. In order to verify the robustness and the superiority of the proposed method, we repeated the ranging experiment 200 times by using the three-point method and the proposed method. The measurement results are shown in Figure 13, and the RMSEs of the proposed method and the three-point method are 0.09 m and 2.44 m, respectively. Thus, the proposed method is effective in compensating for the time-varying vibration error and the nonlinearity error simultaneously, and the estimated range is close to the actual range of the target.

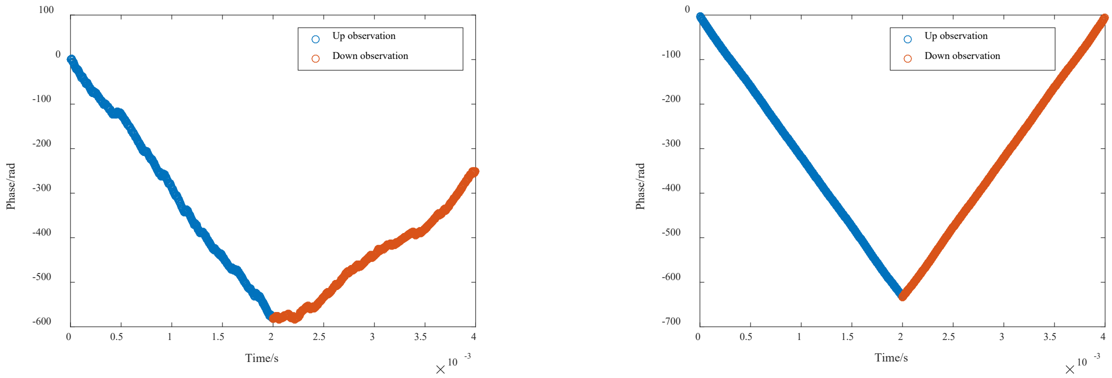

(**a**) (**b**)

Figure 12. Phases of dechirp signals with vibration (**a**) and ideal phases of dechirp signals (**b**).

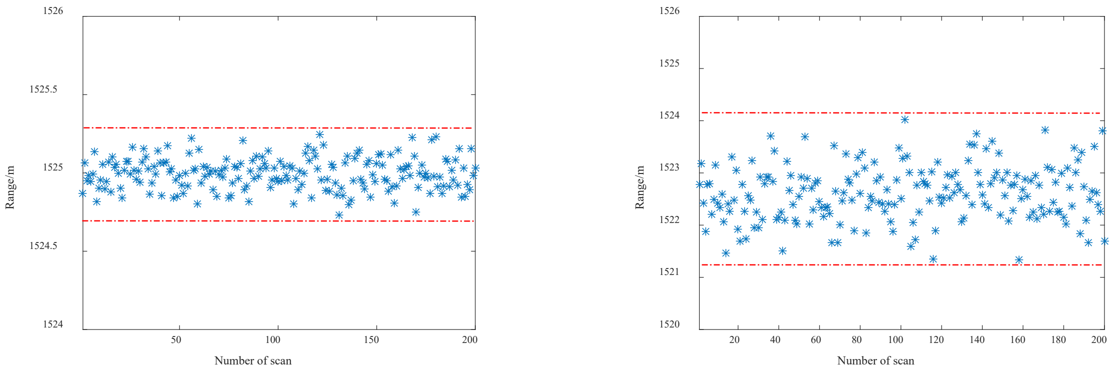

(**a**) (**b**)

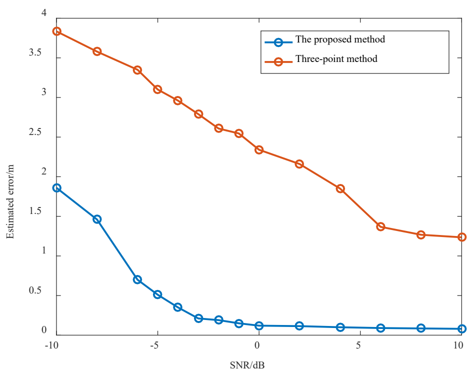

(**c**)

Figure 13. Measurement ranges of the proposed method (**a**) and the three-point method (**b**) in 200−time experiment with SNR of 0 dB; range performance of the two methods with different SNRs (**c**).

To show the robustness of the proposed method against noise, we supplemented a numerical example that compared the proposed method with the three-point method in dealing with noisy signals with different SNRs. We first added two sinusoidal vibration errors with frequencies of 900 Hz and 40 Hz and amplitudes of 2 μm and 50 μm to the ideal dechirp signals. We then added Gaussian white noise with different SNRs to the dechirp signals. We tested the proposed method and the three-point method using the same simulation parameters. The estimated errors for these two methods with different SNRs are shown in Figure 13c, in which the overall estimated errors of the proposed method are smaller than those of the three-point method. As the three-point method uses three specific points to establish mathematical relations that are used to compensate for the vibrations, the jitter introduced by random noise negatively impacts the vibration compensation result. However, the proposed method uses all measurement points in one period and reduces the effect of the random noise to a certain extent. To be specific, the second-order SST can compress noise into granular particles and reduce the interference between noise and effective signals in time-frequency domain. Thus, the proposed method has better performance than the three-point method in dealing with severe vibration and noise.

4.4. Prove the Applicability of the Proposed Method to 3D Imaging

We applied the proposed method to 3D imaging to verify its applicability, and the ideal 3D ground image is shown in Figure 14a. We added a sinusoidal vibration error with amplitude of 20 µm and frequency of 100 Hz and a coupled nonlinearity error to the ideal 3D dechirp signals. The 3D imaging result with coupling errors is shown in Figure 14b, which fluctuates dramatically because of the time-varying coupling errors and the fluctuation affects the target recognition and ground elevation measurement. Then, the proposed method was applied to the 3D dechirp signals to compensate for the time-varying vibration error and the coupled nonlinearity error, and the reconstructed imaging result is shown in Figure 15a. The difference between the reconstructed imaging result of the proposed method and the ideal 3D imaging result is shown in Figure 15b. Figures 14 and 15 show that the estimated imaging result is close to the ideal one, and the differences between the reconstructed and the ideal results are small.

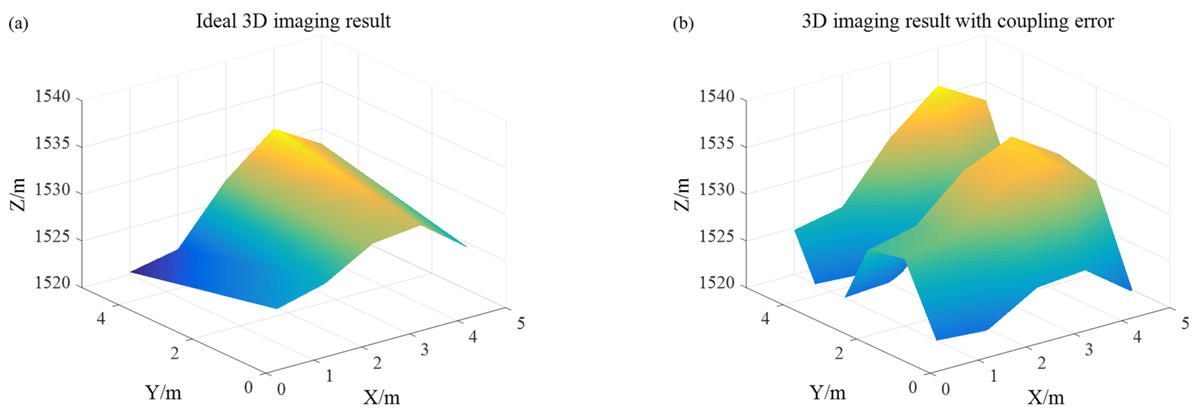

Figure 14. Ideal three dimensional (3D) imaging result (**a**) and 3D imaging result with coupling error (**b**).

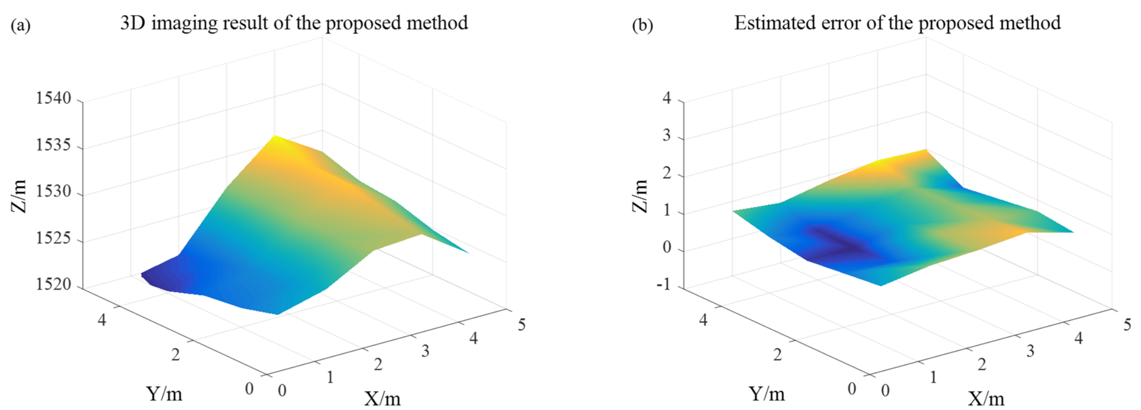

Figure 15. (**a**) Reconstructed 3D imaging result using the proposed method; (**b**) the differences between the reconstructed and the ideal 3D imaging results.

5. Discussion

The vibration compensation methods based on additional lasers in [8–11] can achieve good performance to compensate for vibration errors. However, the additional laser may introduce an asynchronous problem to the ranging result. To solve this problem, we establish a PF model for T-FMCW using an instantaneous ranging model which eliminates the time-varying vibration error from the instantaneous measurement ranges, and the range of target is calculated by using the triangular symmetry relation of T-FMCW. Thus, the proposed method uses only one laser, which can avoid the asynchronous problem between multiple lasers, and thereby simplifies the system configuration. The vibration methods in [13,14] need multiple measurement results and are limited in the application for the 3D imaging Lidar system, as 3D imaging adopts a laser scanner for dynamic range measurement, and the traditional ranging system generally obtains one measurement result in one-period FMCW, which cannot provide enough measurements for the methods in [13,14]. To solve this problem, we extend the traditional ranging model to an instantaneous ranging model based on the second-order SST, which is effective in characterizing the localization of time-varying distributions of the signals in the time-frequency domain. By using the instantaneous ranging model, we can obtain sufficient observation sources to estimate the range of the target. Thus, the proposed method is effective for one-period T-FMCW Lidar signals, which means that it is suitable for 3D imaging.

Besides the vibration error, the nonlinearity error is also an important error source that affects the ranging results. The nonlinearity compensation methods in [18–20] first estimate the nonlinearity errors in the auxiliary channel and then use them to compensate for the nonlinearity by re-sampling. The preliminary nonlinearity compensation in the proposed method is similar to these methods because we also estimate the nonlinearity errors from the auxiliary channel to compensate for the nonlinearity of the measurement channel. However, the estimation methods in above approaches have applicable scope and their results are limited by the accuracy of the estimated nonlinearity errors. If the nonlinearity errors cannot be estimated accurately, the residual nonlinearity errors will degrade the final ranging results. We should note that the preliminary nonlinearity compensation is only a part of the proposed method, and we also use a particle filter to compensate for the disturbance errors and the residual nonlinearity errors. In addition, the second-order SST and particle filter make the proposed method more robust to noise. To be specific, the second-order SST can compress the noise into granular particles in the time-frequency domain, which helps separate the noise from the effective signals in different frequency bands. Second, when the effective signal and noise are in the same frequency band, the particle filter can effectively reduce the interference of noise in the effective signal. The comparison between the proposed method and the envelope detection method as shown in Figure 8 can verify this point.

The methods in [15,16] indicate that we need to consider the coupling effect of vibration and nonlinearity errors on ranging and then compensate for the errors simultaneously. Motivated by the above methods, we derive the impact of vibration error coupled with nonlinearity error on ranging of FMCW Lidar which is the basic of the proposed instantaneous ranging model. Then, the PF model for T-FMCW based on the instantaneous ranging model is proposed to simultaneously deal with coupling errors, and the experiments in Sections 4.2–4.4 show that the proposed method has good performance in compensating for the time-varying errors. Based on the above discussion, we summarize the advantages of the proposed method. First, the method only needs one laser and avoids the asynchronous problem between multiple lasers, and thereby simplifies the system configuration. Second, it can simultaneously compensate for the nonlinearity error and the fast vibration in only one-period T-FMCW Lidar signal, which is supposed to be extremely challenging for the envelope detection method and the three-point method. Finally, the proposed method is robust to noise thanks to the second-order SST and the particle filter.

Recently, synthetic aperture Lidar (SAL) and inverse synthetic aperture Lidar (ISAL) have attracted much attention because they can produce imaging and detecting results with high resolution. However, vibration and nonlinearity are also thorny problems in the applications of SAL and ISAL due to the high frequency of FMCW Lidar signals. Therefore, the applications of the proposed method to SAL and ISAL are our future research directions. In addition, the applicability of the method was proved only by simulation of artificial images and the effect of air turbulence was not considered in the measurements. In our future work, we will apply the proposed method on real data obtained from outside experiment and take air turbulence into consideration.

6. Conclusions

The vibration error coupled with nonlinear modulation error will seriously affect the ranging accuracy of target. In order to reduce the time-varying coupling errors, we first establish an instantaneous ranging model based on second-order SST by using the time-frequency characteristics of dechirp signals. Second, we propose a simultaneous vibration and nonlinearity compensation method based on the PF model using the instantaneous ranges. The proposed method needs only one-period T-FMCW Lidar signal without additional lasers. Numerical tests show that the proposed method can accurately estimate the range of target by compensating for the vibration error coupled with nonlinearity error, and is robust in a noisy environment.

Author Contributions: Conceptualization, M.X. and R.W.; methodology, R.W. and C.L.; validation, R.W., C.L. and S.W.; formal analysis, B.W.; investigation, R.W.; resources, B.W. and M.X.; data curation, C.S. and S.W.; writing—original draft preparation, R.W.; writing—review and editing, R.W. and C.L.; project administration, B.W.; funding acquisition, B.W. All authors have read and agreed to the published version of the manuscript.

Funding: This research was funded by the National Natural Science Foundation of China under grant number 62073306 and the Youth Innovation Promotion Association CAS.

Institutional Review Board Statement: Not applicable.

Informed Consent Statement: Not applicable.

Data Availability Statement: The data presented in this study can be available on request from the corresponding author.

Acknowledgments: The authors would like to express their gratitude to the anonymous reviewers and the associate editor for their constructive comments on the paper.

Conflicts of Interest: The authors declare no conflict of interest.

Abbreviations

The following abbreviations are used in this manuscript:

FMCW	Frequency modulation continuous wave
T-FMCW	Triangular FMCW
second-order SST	Second-order synchrosqueezing transform
PF	Particle filtering
3D	Three dimensional

References

1. Moore, E.D.; McLeod, R.R. Correction of sampling errors due to laser tuning rate fluctuations in swept-wavelength interferometry. *Opt. Express* **2008**, *16*, 13139–13149. [CrossRef]
2. Gao, S.; Hui, R. Frequency-modulated continuous-wave lidar using I/Q modulator for simplified heterodyne detection. *Opt. Lett.* **2012**, *37*, 2022–2024. [CrossRef] [PubMed]
3. Batet, O.; Dios, F.; Comeron, A.; Agishev, R.R. Intensity-modulated linear-frequency-modulated continuous-wave lidar for distributed media: fundamentals of technique. *Appl. Opt.* **2010**, *49*, 3369–3379. [CrossRef]
4. Redman, B.; Ruff, W.; Stann, B.; Giza, M.; Lawler, W.; Dammann, J.; Potter, W. Anti-ship missile tracking with a chirped AM ladar—Update: Design, model predictions, and experimental results. *Def. Secur.* **2005**, *5791*, 330–341. [CrossRef]
5. Karlsson, C.J.; Olsson, F.Å.A. Linearization of the frequency sweep of a frequency-modulated continuous-wave semiconductor laser radar and the resulting ranging performance. *Appl. Opt.* **1999**, *38*, 3376–3386. [CrossRef] [PubMed]

6. Beck, S.M.; Buck, J.R.; Buell, W.F.; Dickinson, R.P.; Kozlowski, D.A.; Marechal, N.J.; Wright, T.J. Synthetic-aperture imaging laser radar: laboratory demonstration and signal processing. *Appl. Opt.* **2005**, *44*, 7621–7629. [CrossRef]
7. Roos, P.A.; Reibel, R.R.; Berg, T.; Kaylor, B.; Barber, Z.W.; Babbitt, W.R. Ultrabroadband optical chirp linearization for precision metrology applications. *Opt. Lett.* **2009**, *34*, 3692–3694. [CrossRef]
8. Kakuma, S.; Katase, Y. Frequency scanning interferometry immune to length drift using a pair of vertical-cavity surface-emitting laser diodes. *Opt. Rev.* **2012**, *19*, 376–380. [CrossRef]
9. Krause, B.W.; Tiemann, B.G.; Gatt, P. Motion compensated frequency modulated continuous wave 3D coherent imaging ladar with scannerless architecture. *Appl. Opt.* **2012**, *51*, 8745–8761. [CrossRef]
10. Yang, H.-J.; Nyberg, S.; Riles, K. High-precision absolute distance measurement using dual-laser frequency scanned interferometry under realistic conditions. *Nucl. Instrum. Methods Phys. Res. Sect A Accel. Spectrom. Detect. Assoc. Equip.* **2007**, *575*, 395–401. [CrossRef]
11. Martinez, J.J.; Campbell, M.A.; Warden, M.S.; Hughes, E.B.; Copner, N.J.; Lewis, A.J. Dual-Sweep Frequency Scanning Interferometry Using Four Wave Mixing. *IEEE Photon Technol. Lett.* **2015**, *27*, 733–736. [CrossRef]
12. Swinkels, B.L.; Bhattacharya, N.; Braat, J.J. Correcting movement errors in frequency-sweeping interferometry. *Opt. Lett.* **2005**, *30*, 2242–2244. [CrossRef]
13. Tao, L.; Liu, Z.; Zhang, W.; Zhou, Y. Frequency-scanning interferometry for dynamic absolute distance measurement using Kalman filter. *Opt. Lett.* **2014**, *39*, 6997–7000. [CrossRef] [PubMed]
14. Jia, X.; Liu, Z.; Tao, L.; Deng, Z.; Deng, L.T.A.Z. Frequency-scanning interferometry using a time-varying Kalman filter for dynamic tracking measurements. *Opt. Express* **2017**, *25*, 25782. [CrossRef] [PubMed]
15. Guo, L.; Huang, Y.; Li, X.; Zeng, X.; Xing, M. A Novel 3-D Imaging Configuration Exploiting Synthetic Aperture Ladar. *Curr. Opt. Photon.* **2017**, *1*, 598–603. [CrossRef]
16. Pierrottet, D.; Amzajerdian, F.; Petway, L.; Barnes, B.; Lockard, G.; Rubio, M. Linear FMCW Laser Radar for Precision Range and Vector Velocity Measurements. *MRS Online Proc. Libr.* **2008**, *1076*. [CrossRef]
17. Ahn, T.-J.; Lee, J.Y.; Kim, D.Y. Suppression of nonlinear frequency sweep in an optical frequency-domain reflectometer by use of Hilbert transformation. *Appl. Opt.* **2005**, *44*, 7630–7634. [CrossRef]
18. Ahn, T.-J.; Kim, D.Y. Analysis of nonlinear frequency sweep in high-speed tunable laser sources using a self-homodyne measurement and Hilbert transformation. *Appl. Opt.* **2007**, *46*, 2394. [CrossRef]
19. Jabbour, C.; Camarero, D.; Nguyen, V.T.; Loumeau, P. A 1 V 65 nm CMOS reconfigurable time interleaved high pass Σ ADC. In Proceedings of the 2009 IEEE International Symposium on Circuits and Systems, Taipei, Taiwan, 24–27 May 2009; pp. 1557–1560. [CrossRef]
20. Yuksel, K.; Wuilpart, M.; Mégret, P. Analysis and suppression of nonlinear frequency modulation in an optical frequency-domain reflectometer. *Opt. Express* **2009**, *17*, 5845–5851. [CrossRef]
21. Lu, C.; Liu, G.; Liu, B.; Chen, F.; Gan, Y. Absolute distance measurement system with micron-grade measurement uncertainty and 24 m range using frequency scanning interferometry with compensation of environmental vibration. *Opt. Express* **2016**, *24*, 30215–30224. [CrossRef] [PubMed]
22. Lu, C.; Xiang, Y.; Gan, Y.; Liu, B.; Chen, F.; Liu, X.; Liu, G. FSI-based non-cooperative target absolute distance measurement method using PLL correction for the influence of a nonlinear clock. *Opt. Lett.* **2018**, *43*, 2098–2101. [CrossRef]
23. Oberlin, T.; Meignen, S.; Perrier, V. Second-Order Synchrosqueezing Transform or Invertible Reassignment? Towards Ideal Time-Frequency Representations. *IEEE Trans. Signal Process.* **2015**, *63*, 1335–1344. [CrossRef]
24. Shan, C.; Tan, T.; Wei, Y. Real-time hand tracking using a mean shift embedded particle filter. *Pattern Recognit.* **2007**, *40*, 1958–1970. [CrossRef]
25. Iiyama, K.; Matsui, S.-I.; Kobayashi, T.; Maruyama, T. High-Resolution FMCW Reflectometry Using a Single-Mode Vertical-Cavity Surface-Emitting Laser. *IEEE Photon Technol. Lett.* **2011**, *23*, 703–705. [CrossRef]
26. Anghel, A.; Vasile, G.; Cacoveanu, R.; Ioana, C.; Ciochina, S. Short-Range Wideband FMCW Radar for Millimetric Displacement Measurements. *IEEE Trans. Geosci. Remote. Sens.* **2014**, *52*, 5633–5642. [CrossRef]
27. Stove, A.G. Linear FMCW radar techniques. *Radar Signal Process. IEE Proc. F* **1992**, *139*, 343. [CrossRef]
28. Ding, Z.; Yao, X.S.; Liu, T.; Du, Y.; Liu, K.; Jiang, J.; Meng, Z.; Chen, H. Compensation of laser frequency tuning nonlinearity of a long range OFDR using deskew filter. *Opt. Express* **2013**, *21*, 3826–3834. [CrossRef]
29. Song, N.; Yang, D.; Lin, Z.; Ou, P.; Jia, Y.; Sun, M. Impact of transmitting light's modulation characteristics on LFMCW Lidar systems. *Opt. Laser Technol.* **2012**, *44*, 452–458. [CrossRef]
30. Barber, Z.W.; Babbitt, W.R.; Kaylor, B.; Reibel, R.R.; Roos, P.A. Accuracy of active chirp linearization for broadband frequency modulated continuous wave ladar. *Appl. Opt.* **2010**, *49*, 213–219. [CrossRef] [PubMed]
31. Meta, A.; Hoogeboom, P.; Ligthart, L.P. Signal Processing for FMCW SAR. *IEEE Trans. Geosci. Remote. Sens.* **2007**, *45*, 3519–3532. [CrossRef]
32. Jia, X.; Liu, Z.; Deng, Z.; Deng, W.; Wang, Z.; Zhen, Z. Dynamic absolute distance measurement by frequency sweeping interferometry based Doppler beat frequency tracking model. *Opt. Commun.* **2019**, *430*, 163–169. [CrossRef]
33. Meignen, S.; Oberlin, T.; McLaughlin, S. A New Algorithm for Multicomponent Signals Analysis Based on SynchroSqueezing: with an Application to Signal Sampling and Denoising. *IEEE Trans. Signal Process.* **2012**, *60*, 5787–5798. [CrossRef]

34. Wang, S.; Chen, X.; Cai, G.; Chen, B.; Li, X.; He, Z. Matching Demodulation Transform and SynchroSqueezing in Time-Frequency Analysis. *IEEE Trans. Signal Process.* **2014**, *62*, 69–84. [CrossRef]
35. Carmona, R.; Hwang, W.L.; Torresani, B. Multiridge detection and time-frequency reconstruction. *IEEE Trans. Signal Process.* **1999**, *47*, 480–492. [CrossRef]
36. Halmos, M.J.; Klotz, M.J.; Bulot, J.P. Optical Delay Line to Correct Phase Errors in Coherent LADAR. U.S. Patent US20060279723A1, 18 March 2008.
37. Zhang, L.; Gao, Y.; Liu, X. Fast channel phase error calibration algorithm for azimuth multichannel high-resolution and wide-swath synthetic aperture radar imaging system. *J. Appl. Remote Sens.* **2017**, *11*, 035003. [CrossRef]